Medium-resolution studies of extreme ultraviolet emission from N_2 by electron impact: Vibrational perturbations and cross sections of the $c_4'\,^1\Sigma_u^+$ and $b'\,^1\Sigma_u^+$ states

Joseph M. Ajello, Geoffrey K. James, and Brian O. Franklin
Jet Propulsion Laboratory, California Institute of Technology, Pasadena, California 91109

Donald E. Shemansky
Lunar and Planetary Laboratory, University of Arizona, Tucson, Arizona 85712
(Received 6 April 1989)

We have studied in a crossed-beam experiment the electron-impact-induced fluorescence spectrum of N_2 in the extreme ultraviolet (euv) at a spectral resolution of up to 0.03 nm. The optically thin experiment allowed us to obtain the highest-resolution electron-impact emission spectrum of the Rydberg and valence states of N_2. The spectral measurements provide the emission cross sections of each of the vibrational transitions of the $c_4'\,^1\Sigma_u^+ \rightarrow X\,^1\Sigma_g^+$ Carroll-Yoshino band system and the $b'\,^1\Sigma_u^+ \rightarrow X\,^1\Sigma_g^+$ Birge-Hopfield-II band system. The $c_4'\,^1\Sigma_u^+$ and $b'\,^1\Sigma_u^+$ states strongly perturb one another by homogeneous configuration interactions. This perturbation leads to vibrational-excitation cross sections whose dependence on v' is quite different from the variation of the unperturbed Franck-Condon factors. The laboratory cross sections were measured from 10 to 400 eV. A modified Born approximation analytic model is given for the $c_4'\,^1\Sigma_u^+$ and $b'\,^1\Sigma_u^+$ vibrational-excitation cross sections. The modified Born approximation analysis leads to accurate band-system oscillator strengths. The emission cross section for the $c_4'(0)$ level is found to be the same to within 10% by the relative flow technique and the theoretical excitation cross section using the modified Born approximation and the published $c_4'(0,0)$ oscillator strength. The relative emission cross section for each of the vibrational levels ($v'=0$–4,6) of the $c_4'\,^1\Sigma_u^+$ state closely agrees with the relative excitation cross section from electron-energy-loss experiments. Predissociation for the vibrational levels of the $c_4'\,^1\Sigma_u^+$ state is estimated to be less than 10%. On the other hand, a comparison of emission and excitation cross sections shows that the $b'\,^1\Sigma_u^+$ state is 84% predissociated and that the predissociation yield generally increases with vibrational quantum number. In addition, we have measured at low resolution (0.5 nm) the cross section of the atomic dissociation fragments (N I,N II,N III) from 40 to 102 nm, and we have measured at medium resolution (0.05 nm) the emission cross section of the $c_4\,^1\Pi_u$, $c_5'\,^1\Sigma_u^+$, $c_5\,^1\Pi_u$, and $c_6'\,^1\Sigma_u^+ \rightarrow X\,^1\Sigma_g^+(0,0)$ transitions. The emission and excitation cross sections represent a substantial improvement in the available data base. Previous electron-impact measurements were hampered by an incorrect value of the Lyman-α standard cross section, uncertain band-system oscillator strengths, incorrect identification of strongest spectral features, and unresolved structure. This problem has led aeronomers of the Earth's upper atmosphere to overestimate the euv photon flux and predissociation yields from Rydberg and valence states of N_2 in the photoelectron-excited dayglow and aurora by a factor of 2.

INTRODUCTION

An understanding of the configuration interaction[1] between the Rydberg and valence state of N_2 requires high-resolution measurements of intensities by either electron energy loss or optical emission techniques in a single-scattering experiment. The highest-resolution experiment to date was a 10-meV electron-energy-loss experiment conducted 20 years ago by Geiger and Schroder.[2] In this paper we report extreme ultraviolet (euv) measurements of the emission spectrum of N_2 at 0.03-nm (4-meV) resolution produced by electron impact at 20 and 100 eV. By this means we can unambiguously identify and measure the emission cross sections for the $c_4'\,^1\Sigma_u^+ \rightarrow X\,^1\Sigma_g^+$ and $b'\,^1\Sigma_u^+ \rightarrow X\,^1\Sigma_g^+$ band systems referred to as the Carroll-Yoshino and Birge-Hopfield-(BH) II bands. A comparison of the electron-scattering experiment intensities and the emission experiment intensities presented here provides estimates of predissociation and emission yields.

We will report on the $b\,^1\Pi_u \rightarrow X\,^1\Sigma_g^+$ Birge-Hopfield I band system in another paper.[3] This is a logical separation of these band systems based on the homogeneous interaction that exists between pairs of states of Σ and Π symmetry. The homogeneous interaction between the b' valence state and c_4' Rydberg state (also c_5' state) is so strong that it is not localized to a few rotational levels but rather globally affects all the rotational levels in a vibrational level.[4–8] This interaction is referred to as a homogeneous vibrational perturbation.[9] It arises because of the near-energy resonances between vibrational levels. Most vibrational levels in both states are affected in this way. In emission observable intensity differences are found from direct excitation intensities predicted by Franck-Condon factors based on diabatic potential curves. This intensity variation is in addition to the ener-

gy shifts of rotational levels. The anomalous intensity variation in the electron scattering experiment of Geiger and Schroder has been explained by Stahel, Leoni, and Dressler[10] as a quantum-mechanical interference effect of the interacting states. Vibrational levels borrow population at the expense of the levels to which they are energetically resonant. The emission experiment presented here is much more difficult to model because not only is the upward excitation process affected by the interference effect, but the downward emission branching ratios are complicated because of both interference effects to all lower levels and predissociation. In general, cascading is not important in determining vibrational populations for the two states.[11,12] Thus any differences in vibrational intensities noted between experiment and the Franck-Condon approximation are due to both avoided adiabatic curve crossings, i.e., mixing of the unperturbed wave functions and predissociation.[13,14] We show that for the vibrational levels of the c_4' state predissociation is small ($<10\%$).

Diabatic and adiabatic potential curves for these states have been recently calculated by Stahel, Leoni, and Dressler.[10] In principle, a synthetic emission spectrum for the adiabatic potential curves can be developed based on the results of Stahel, Leoni, and Dressler. The difference between the synthetic and experimental spectrum can be attributed to predissociation. However, substantial differences exist between the electron-scattering energy loss model developed by these authors and the data. Thus a high-resolution emission spectrum is a prime data set for testing perturbation theory developed by Stahel, Leoni, and Dressler[10] and Lefebvre-Brion and Field.[15]

Absorption studies at high resolution by Yoshino, Carroll, and co-workers have laid the ground work for cataloging and interpreting the irregularities in the vibrational levels of the b' and c_4' states.[4-8] They have shown that other Rydberg states (e.g., c_5' also called e are also involved in the vibrational perturbations of the b' and c_4' states. To a lesser degree, heterogeneous rotational perturbations are simultaneously observed in the various Rydberg complexes, e.g., $c_4'-c_3$.[5] The irregularities in position and intensity can be best explained by multilevel perturbations.[16]

An important work accurately identifying the features found in the N_2 euv emission spectrum was recently published by Roncin, Launay, and Yoshino[17] from experiments performed at the Meudon Observatory. Their low-pressure discharge lamp spectrum probed the euv spectrum of N_2 over the wavelength range 85–105 nm at a resolution of 0.008 nm and a gas pressure of 0.01 Torr, laying to rest any claims of strong predissociation for these states. At this resolution sharp features were observed to $v'=19$ for the b' state and $v'=6$ for the c_4' state. Our work at 0.03-nm resolution and a pressure of 5×10^{-6} Torr complements the Meudon results by observing the resonance bands ($v''=0$) for the c_4' and b' states. The resonance bands are very important for these two-band systems since most of the emission cross section for the electronic states is tied up in the vibrational resonance transitions. In fact, the $c_4'(0,0)$ band contains roughly 62% of the emission-excitation cross section of the c_4' band system and half the intensity in the euv (80–102 nm).

Previous attempts at analyzing the electron-impact emission spectrum of N_2 in the euv have lead to misinformation concerning cross sections and predissociation rates. For example, the work of Zipf and McLaughlin[18] report the c_4' state as virtually 100% predissociated for $v'>3$. On the contrary, we find the predissociation for these levels as less than 10%. Much of this misinformation arose for lack of accurate identifications of vibrational bands and erroneous calibration standards available at the time. In addition, reanalysis of this original data now is not favorable because in some cases the spectra were optically thick or at insufficient resolution.[18-21] These authors studied a few of the bands and dissociative NI II emissions found in the euv.[18-21]

We extend the previous work by measuring the cross sections for all features at low resolution (0.5 nm) at 200 eV. For the wavelength region encompassing the c_4' and b' systems from 85 to 102 nm we obtained higher-resolution measurements at 0.05 and 0.03 nm. By "counting all the photons" from the b' and c_4' vibrational levels, we avoid any unnecessary extrapolations to the entire band system from the measurements of only a few vibrational bands, a technique often employed in calculating electronic emission cross sections. In addition, we measure excitation functions for $c_4'(0,0)$ and $b'(16,0)$ transitions. Results from analysis of the excitation function by the modified Born approximation[22] using the measured oscillator strength[23,24] of the c_4' (0,0) band can be compared to results from the relative-flow technique[25] using the new Lyman-α cross section from dissociative excitation of H_2.[26,27] The ratio of the emission cross section to the excitation cross section gives the emission yield.

The subject of the amount of predissociation of the b' and c_4' states has had an interesting and long history. Initially, the first emission results at high resolution by Tilford and Wilkinson,[28] and Wilkinson and Houk[29] interpreted rotational intensity anomalies actually caused by self-absorption as evidence for strong predissociation. This effect has recently been pointed out by Roncin Launay, and Yoshino.[17] The only current spectroscopic evidence for strong predissociation in either the b' or c_4' states is from the high-resolution (~5 mA) absorption spectra of Carroll, Collins, and Yoshino[5] showing rotational diffuse transitions in $v'=20$, 21, 22 of the b' state and the high-resolution emission spectra of Roncin, Launay, and Larzilliere[30] showing a sharp breaking off beyond $J=12$ for the c_4' (6) level. The strong predissociations arise from a singlet state(s) derived from the $^2D^0+{}^2D^0$ atomic products formed at the 14.3-eV limit between $v'=19$ and 20 of the b' state. On the other hand, the work of Zipf and McLaughlin[18] for the b' state indicates a substantial 83% predissociation yield for $v'<20$. The Lyman-α cross section used by this group for this study was about 61% too high.[31] Thus the predissociation yield would be expected to approach 90% with a correction to the emission cross section. The first direct evidence for predissociation from the b' state for $v'<20$ arises from the measurement of the kinetic energy of the

$N(^2D^\circ)$ and $N(^2P^\circ)$ product atoms from predissociation of $v'=16,17$. For this study the technique of photofragment spectroscopy was employed by Helm and Cosby.[32] Thus predissociation rates appear to be in the range that "breaking off the bands in emission" would be definitive evidence for the strength. However, the chaotic nature of the N_2 euv vibrational emission spectrum due to interference effects would make such interpretations difficult. Lefebvre-Brion and Field[15] report in their monograph discussion of N_2 $b'\sim c_4'$ perturbations that "weak predissociations cannot be ruled out, but are not needed to account for present experimental observations." Thus the terms "weak" and "strong" predissociations often used in the literature have to be viewed with caution when interpreting N_2 euv spectrum. We show that all the predissociation estimates can be reconciled by referring to a weak predissociation as a predissociation process with a yield of less than 90–99 %.

Electron-energy-loss measurements have been made by Lassettre[33] and Chutjian, Cartwright, and Trajmar.[34] Chutjian, Cartwright, and Trajmar measured the cross sections of the 12–14-eV Rydberg and valence states including the c_4' and b' states at $\sim$50-meV resolution.

This work represents our first measurement with a medium-resolution (0.02-nm) vacuum ultraviolet (vuv) spectrometer operated in tandem with an electron collision chamber. A second euv paper is planned.[3] The far ultraviolet (fuv) work was described in a paper by Ajello and Shemansky[35] and was an examination of the cross section and threshold effects of the Lyman-Birge-Hopfield (LBH) band system. This work is also part of a continuing program to measure cross sections of species of fundamental importance to atomic and molecular physics and to atmospheric and astrophysical physics in the vuv. The calibration technique[36] employed in calibrating the spectrometer in the N_2 measurements is described by Ref. 36. In addition, recent papers have described the emission cross sections of He,[22] H_2,[26,37] O_2,[38] C_2H_2, and CH_4.[27] The latter paper[27] is the source of our present Lyman-α cross section.

N_2 is the most abundant gas in the lower thermosphere of the Earth[39] and in the upper atmosphere of the Saturnian moon, Titan,[40] at the altitude where energy deposition processes maximize. euv emissions have been observed from both objects. In the case of the Earth, N_2 emissions are masked by strong atomic O emissions and redistribution of resonance radiation energy by multiple scattering into other bands or predissociation.[41–44] However, before these multiple-scattering processes can be modeled by aeronomers the single-scattering process observed in the laboratory has to be understood. This is the goal of the present paper. In the ensuing sections we discuss the laboratory technique employed for calibration, cross-section, and spectral measurements. We then describe in detail the low-spectral-resolution measurements of the entire euv (40–120 nm), followed by detailed discussions of the c_4' and b' band systems.

EXPERIMENTAL APPARATUS AND CALIBRATION

The apparatus used in the present measurements is shown in Fig. 1. It consists of an electron-impact collision chamber in tandem with a uv spectrometer. For spectral scans the instrument is operated in the crossed-beam mode in which a magnetically collimated electron beam (2–400 eV) is crossed with a gas beam formed by a capillary array at a background pressure that can be varied from 5×10^{-8} to 3×10^{-4} Torr. This geometry establishes a point emission source ($\sim$1 mm^3) collision region. Optimum alignment of the gas beam with respect to the electron beam is achieved by three-axis manipulation of the capillary array. Alternatively, a uniform static gas sample can be admitted to the chamber over the same pressure range forming a line-source collision region approximately 1.8 cm$\times$1 mm for excitation-function measurements. Emitted photons are detected at

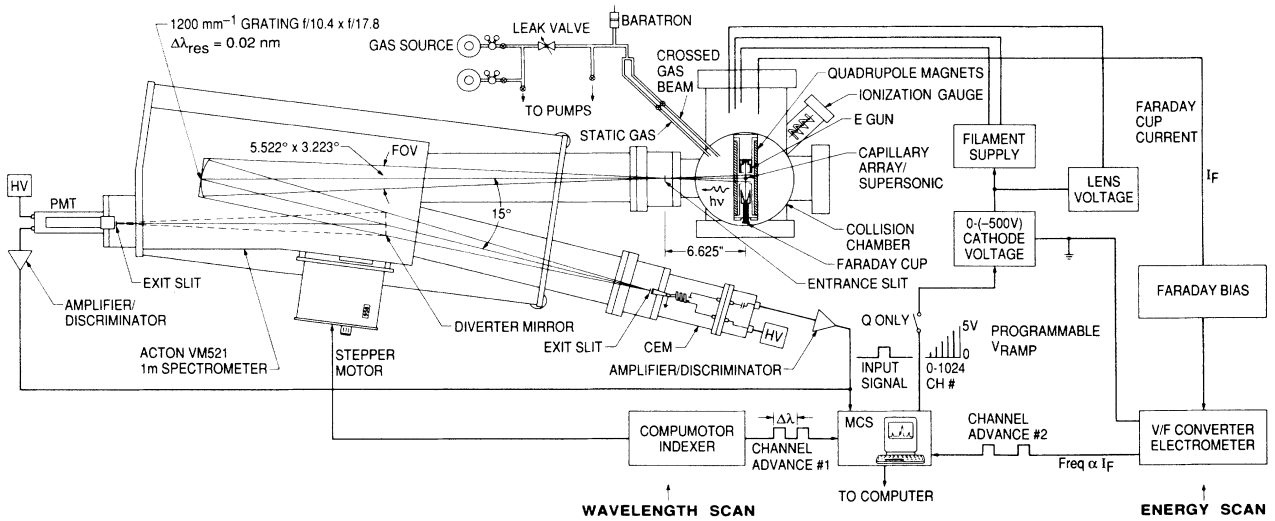

FIG. 1. Scale drawing and electronic schematics of 1-m vuv monochromator in tandem with electron-impact collision chamber. Spectral measurements are taken in the crossed-beam mode and cross-section excitation functions are made in the static-gas mode.

90° by an Acton VM-521 1.0-m vacuum spectrometer. No corrections for polarization of the radiation are made. Polarization of the radiation is considered to be small where many rotational states contribute to a vibrational band for an excited molecule.

The electron-beam source has been described in detail by Ajello *et al.*[36] In brief, thermionic electrons produced by heating a tungsten filament are extracted from the filament region by a Pierce electrode and extractor lens combination and accelerated or decelerated by an aperture lens or anode to achieve the final energy (2–400 eV). The electron beam is collimated by the axially symmetric magnetic field (120 G) produced by a permanent magnet quadrupole configuration surrounding the entire electron gun. A Faraday cup designed to minimize backscattered secondary electrons is used to monitor the electron-beam current. The ability of the Faraday cup to prevent the escape of secondary electrons generated in the cup is essential for accurate excitation function measurements and has been verified by measurement of the N_2 ($a\ ^1\Pi_g \rightarrow X\ ^1\Sigma_g^+$) optically forbidden LBH excitation function.[35] The energy spread of the beam is equal to the thermal energy (0.3 eV) and the absolute energy scale for excitation-function measurements is estimated to be accurate to approximately 0.5 eV by comparison with the He I resonance line appearance potential at 21.2 eV.

The Acton VM-521, 1.0-m spectrometer operates at near-normal incidence. The optical system has a horizontal aperture ratio of $f/10.4$ with a 1200-lines/mm osmium coated grating covering the wavelength range 30–325 nm. With suitable gratings and detectors the spectrometer is capable of operating in the wavelength range from 30 nm to 1.3 μm. Dual exit ports enable either of two different detectors to be indexed using a diverter mirror and without breaking vacuum. For the present measurements a channeltron electron multiplier (CEM) is installed on exit port 1. The channeltron detector has a useful spectral range from 40 to 125 nm. A photomultiplier with a CsTe photocathode and MgF_2 window is installed on exit port 2 for use in the wavelength range 115–300 nm. The spectrometer has a dispersion of 0.83 nm/mm and a measured resolution of 0.03 nm full width at half maximum (FWHM) with 20-μm entrance and exit slit widths. This represents a 13-fold improvement in resolution compared to the 0.2-m spectrometer previously used to obtain electron-impact-induced N_2 emission spectra (50–190 nm) at 0.4-nm resolution (see Fig. 1 of Ajello and Shemansky[35] and Fig. 4 of this work, to be discussed in the next section). The improved resolution is essential to separate the many blended spectral components in this wavelength range as demonstrated in Table I.

The spectrometer is interfaced to a multichannel scalar and computer and is completely automated. Wavelength scans are made using a Compumotor indexer to provide channel advance pulses for the multichannel scalar and to increment a stepper motor which rotates the diffraction grating drive screw. For excitation-function measurements the signal measured by the multichannel scalar is automatically normalized in real time to the electron-beam current at each energy. A V-to-F converter produces a frequency proportional to the Faraday-cup current. After a given number of cycles the V-to-F converter generates an external channel advance pulse for the multichannel scalar which then increments the output voltage ramp used to control the electron-beam energy. Thus the signal accumulated at each electron-beam energy corresponds to the same integrated beam current.

The relative intensity calibration of the optical system and detector with wavelength is determined by at least two procedures in each wavelength region. These calibration methods have been described in detail by Ajello *et al.*[36,37] for the wavelength range 50–230 nm. In brief, electron-excited spectra of reference gases He, H_2, N_2, and Ar are used as calibration sources in which the relative emission intensity as a function of wavelength depends directly on the fundamental constants (transition probabilities and collision strengths) for the molecular or atomic system. The relative spectral sensitivity of the spectrometer system is established by comparing the strengths of the molecular or atomic features measured with synthetic models. These laboratory measurements together with the spectroscopic models allow the vuv spectrum from H_2 Rydberg series and N_2 LBH bands to serve as relative intensity calibration standards in the 80–230-nm range with a 10% accuracy of the model fit to the two sets of data. A somewhat larger uncertainty of 20% is given for the range from 80 to 90 nm.[36] The relative calibration curve for the spectrometer used in the present work from 80 to 125 nm was obtained from measurements of H_2 Rydberg band systems and Ar I and Ar II multiplets[36] and is shown in Fig. 2. At lower wavelengths (40–80 nm) the $n\ ^1P^\circ$ $n=2,3,4$ Rydberg series of He and

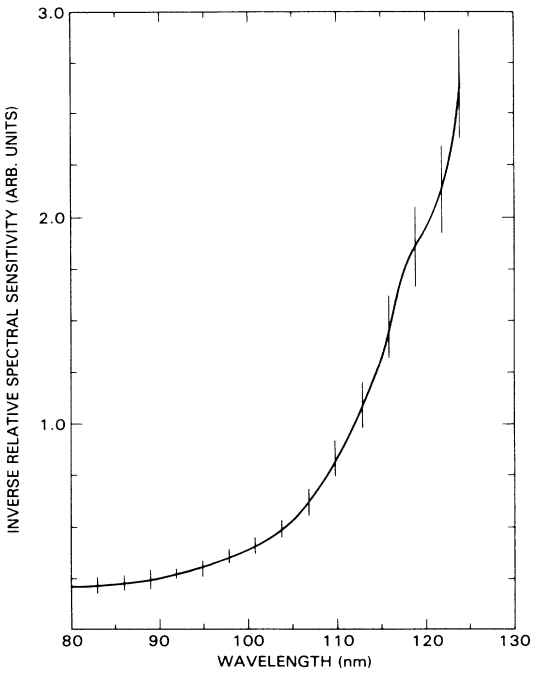

FIG. 2. Instrumental inverse sensitivity is shown as a function of wavelength. It is determined by three calibration techniques described in Ajello *et al.* (Ref. 36). Error bars are indicated as vertical lines.

TABLE I. Emission cross section of N_2 at 100 and 200 eV. + denotes the unperturbed theoretical intensity $< 10^{-4}$ of the band system; * denotes the unperturbed theoretical intensity $> 10^{-2}$ of the band system. No entry for features 1,6,8 unresolved wavelength peak.

Feature No.	Species	Wavelength (nm)	Term	Observed peak wavelength (nm)	Integrated wavelength interval (nm)	Cross section at 200 eV (10^{-19} cm^2)	Cross section at 100 eV (10^{-19} cm^2)	Other measurements at 200 eV (100 eV) (10^{-19} cm^2)
1	N II	45.3257	$g\,^3P$–$^3D^\circ$			< 0.2		
	N II	45.3340	$g\,^3P$–$^3D^\circ$					
2	N II	47.3180–47.3473	$g\,^3P$–$^1P^\circ$	47.6	47.1–47.9	0.27		
	N II	47.4493–47.5884	$g\,^3P$–$^3P^\circ$, $^3D^\circ$					
3	N II	48.5062	^1D–$^1P^\circ$	48.6	48.2–49.5	0.18		
	N II	48.5849	^1D–$^1F^\circ$					
4	N II	50.5411–50.5746	$g\,^3P$–$^1P^\circ$	50.9	50.2–52.1	0.45		
	N II	50.5986–50.6153	$^5S^\circ$–^5P					
	N II	50.8484–50.9006	$g\,^3P$–$^3P^\circ$					
	N II	51.0758	^1D–$^1F^\circ$					
	N II	51.3849	^1D–$^1F^\circ$					
5	N II	52.5983–52.6345	$g\,^3P$–$^1P^\circ$	53.2	52.2–54.1	1.96		
	N II	52.9355–52.9867	$g\,^3P$–$^3P^\circ$					
	N II	53.3511–53.3815	$g\,^3P$–$^3D^\circ$					
	N II	53.4637	$g\,^3P$–$^1D^\circ$					
	N II	53.4872	$g\,^3P$–$^1D^\circ$					
6	N II	55.9762	^1S–$^1P^\circ$			< 0.2		
7	N II	57.2069	^1D–$^1P^\circ$	57.4	56.8–57.9	0.98		
	N II	57.4650	^1D–$^1F^\circ$					
8	N II	58.2156	^1D–$^1D^\circ$			< 0.2		
9	N II	62.9167–62.9670	$^5S^\circ$–^5P	63.4	62.7–64.2	0.90		
	N I	63.1624	$g\,^4S^\circ$–^4P					
	N II	63.5197	^1S–$^1P^\circ$					
	N II	63.9082	$^5S^\circ$–^3P					
	N II	63.9368	$^5S^\circ$–^3P					
	N II	64.0121	^1S–$^3P^\circ$					
10	N II	64.4634–64.5178	$g\,^3P$–$^3S^\circ$	64.4	64.2–65.3	0.63		
	N I	64.7505	$g\,^4S^\circ$–^4P					
11	N II	66.0286	^1D–$^1P^\circ$	65.9	65.6–66.5	0.45		
12	N II	67.0296–67.0884	$g\,^3P$–$^1P^\circ$	67.1	66.5–68.1	6.3		1.7[a]
	N II	67.1016–67.2001	$g\,^3P$–$^3P^\circ$					
13	N III	68.4996–68.6335	$g\,^2P^\circ$–^2P	68.6	68.1–69.3	0.32		
14	N II	74.5841	^1S–$^1P^\circ$	74.6	74.3 –75.5	2.9		1.0[a]
	N II	74.6984	^1D–$^1P^\circ$					1.5[b]
	N II	74.8369	^1D–$^3P^\circ$					
15	N II	77.5965	^1D–$^1D^\circ$	77.6	77.3–78.6	1.9		0.7[a] 1.1[b]
16				83.53	83.2–84.2	0.90	0.57	
A	N_2	83.3747	$c_6'(0,0)$	83.39	83.33–83.43		0.02	
B	N_2	83.5144	$c_5(0,0)$	83.53	83.43–83.60		0.37	
C	N II	83.6187–83.6837	$^3D^\circ$–^3P	83.64	83.60–83.71		0.12	
D	N_2	84.1992	$c_4'(7,0)$	84.19	84.05–84.28		0.062	
17				85.7& 86.4	84.8–87.1	3.9	4.67	
A	N_2	85.026	$c_6'(0,1)$	85.05	84.98–85.06		0.10	

TABLE I. (*Continued*).

Feature No.	Species	Wavelength (nm)	Term	Observed peak wavelength (nm)	Integrated wavelength interval (nm)	Cross section at 200 eV (10^{-19} cm^2)	Cross section at 100 eV (10^{-19} cm^2)	Other measurements at 200 eV (100 eV) (10^{-19} cm^2)
B	N_2	85.18	$c_5(0,1)$	85.19	85.10–85.27		0.07	
C	N_2	85.6115	$c_4'(6,0)^+$	85.65	85.55–85.91		0.88	
	N_2	85.7011	$b'(19,0)^+$					
	N I	85.777	$g\,^4S°–^4P$					
	N II	85.8376	$^1S–^1P°$					
	N I	85.880	$g\,^4S°–^4P$					
D	N I	86.004–86.115	$g\,^4S°–^4S,^4P$	86.09	85.98–86.16		0.16	
	N II	86.0205	$^1S–^3P°$					
	N_2	86.0511	$b'(18,0)$					
E	N I	86.214	$g\,^4S°–^4P$	86.37	86.18–86.43		0.54	
	N I	86.291	$g\,^4S°–^4P$					
	N I	86.299	$g\,^4S°–^4P$					
	N_2	86.3158	$c_5'(0,0)$					
F	N I	86.4868	$g\,^4S°–^4D$	86.54	86.43–86.65		2.33	
	N_2	86.53	$c_4\,^1\Pi_u(0,0)$					
	N I	86.565	$^2P°–^4P$					
	N I	86.595	$g\,^4S°–^4P$					
G	N_2	86.671	$b'(17,0)$	86.74	86.65–86.82		0.19	
	N_2	86.723	$c_6'(0,2)$					
H	N I	86.94–87.04	$g\,^4S°–^4P,^2F,^4F$	86.94	86.86–87.04		0.40	
18				87.3	87.0–87.9	3.6	4.10	
A	N_2	87.0755	$c_4'(5,0)^+$	87.16	87.04–87.29		2.14	
	N_2	87.1426	$b'(16,0)$*					
B	N_2	87.354	$c_4'(6,1)^+$	87.35	87.29–87.44		0.89	
C	N_2	87.449	$b'(19,1)^+$	87.59	87.44–87.89		1.07	
	N I	87.4934–87.5791	$g\,^4S°–^4P,^2D,^4D,^2P$					
	N_2	87.5885	$b'(15,0)$*					
	N I	87.6066–87.6987	$g\,^4S°–^4P,^4F,^2P$					
19				88.8	87.9–89.9	4.7	5.60	
A	N_2	88.0753	$b'(14,0)$	88.12	87.97–88.28		0.57	
	N_2	88.091	$c_5'(0,1)$*					
B	N_2	88.311	$c_4(0,1)^+$	88.31	88.28–88.46		0.29	
	N_2	88.467	$c_6'(0,3)$					
C	N I	88.5380	$g\,^4S°–^2D$	88.70	88.46–88.99		2.98	
	N I	88.5387	$g\,^4S°–^2D$					
	N I	88.5527	$g\,^4S°–^2D$					
	N_2	88.5673	$b(13,0)$					
	N I	88.5656	$g\,^4S°–^4D$					
	N I	88.5668	$g\,^4S°–^4D$					
	N I	88.5704	$g\,^4S°–^4D$					
	N I	88.5973	$g\,^4S°–^4P$					
	N_2	88.603	$c_3(4,0)$					
	N I	88.6226	$g\,^4S°–^4P$					
	N I	88.6332	$g\,^4S°–^4P$					
	N I	88.6428	$g\,^4S°–^2F$					
	N I	88.6465	$g\,^4S°–^2P$					
	N I	88.6517	$g\,^4S°–^2P$					
	N_2	88.6777	$c_4'(4,0)^+$					
	N I	88.6829	$g\,^4S°–^4F$					
	N I	88.6840	$g\,^4S°–^4F$					
	N I	88.7016	$g\,^4S°–^2P$					

TABLE I. (*Continued*).

Feature No.	Species	Wavelength (nm)	Term	Observed peak wavelength (nm)	Integrated wavelength interval (nm)	Cross section at 200 eV (10^{-19} cm^2)	Cross section at 100 eV (10^{-19} cm^2)	Other measurements at 200 eV (100 eV) (10^{-19} cm^2)
	N I	88.7375	$g\,^4S°–^2P$					
	N I	88.7457	$g\,^4S°–^4P$					
	N I	88.8022	$g\,^4S°–^4P$					
	N I	88.8372	$g\,^4S°–^4P$					
	N_2	88.8819	$b(16,0)$					
	N_2	88.949	$b'(16,1)^+$					
D	N_2	89.0962	$b'(12,0)$*	89.13	88.99–89.36		1.27	
	N_2	89.146	$c_4'(6,2)^+$					
	N_2	89.245	$b'(19,2)$					
	N_2	89.3872	$b(15,0)$					
E	N_2	89.6208	$b'(11,0)$*	89.65	89.55–89.80		0.49	
	N_2	89.626	$b'(18,2)$					
20				90.9	89.0–91.3	5.2	6.34	
A	N II	90.0724–90.1626	$^3D°–^3P$	90.11	90.01–90.22		0.38	
	N_2	90.108	$o_3(4,1)$					
	N_2	90.1369	$b'(10,0)$					
B	N_2	90.253	$c_3(3,0)$	90.38	90.22–90.46		0.50	
	N_2	90.303	$b'(17,2)$*					
	N_2	90.3698	$c_4'(3,0)^+$					
	N II	90.3962	$^3D°–^3D$					
	N_2	90.434	$b'(13,1)$*					
C	N_2	90.4740	$b(13,0)$	90.61	90.46–90.73		2.62	
	N II	90.4855	$^3D°–^3D$					
	N I	90.5223	$g\,^4S°–^2D$					
	N II	90.5286	$^3D°–^3D$					
	N I	90.5411	$g\,^4S°–^2D$					
	N_2	90.549	$c_4'(4,1)^+$					
	N I	90.5787	$g\,^4S°–^4D$					
	N I	90.5839	$g\,^4S°–^4D$					
	N I	90.5916	$g\,^4S°–^4D$					
	N I	90.6206	$g\,^4S°–^4P$					
	N I	90.6433	$g\,^4S°–^4P$					
	N I	90.6617	$g\,^4S°–^4P$					
	N I	90.6730	$g\,^4S°–^2F$					
	N I	90.7609	$g\,^4S°–^2P$					
	N I	90.7275	$g\,^4S°–^2P$					
D	N I	90.7337	$g\,^4S°–^4F$	90.83	90.73–90.90		1.15	
	N_2	90.7462	$b'(9,0)$					
	N I	90.7485	$g\,^4S°–^4F$					
	N_2	90.808	$b'(16,2)$*					
	N I	90.823 32	$g\,^4S°–^2P$					
	N I	90.879 58	$g\,^4S°–^2P$					
E	N I	90.969 76 ST	$g\,^4S°–^4P$	91.01	90.88–91.19		1.69	
	N_2	90.985	$b'(12,1)$*					
	N_2	90.989	$c_4'(6,3)^+$					
	N I	91.027 85 ST	$g\,^4S°–^4P$					
	N_2	91.0489	$b(12,0)$					
	N I	91.064 56 ST	$g\,^4S°–^4P$					
21				91.7	91.3–92.6	9.5	6.86	2.9[a] 4.4[b] 8.3[f]
A	N_2	91.533	$b'(11,1)$	91.67	91.50–91.74		5.71	
	N II	91.5612	$g\,^3P–^3P°$					

TABLE I. (*Continued*).

Feature No.	Species	Wavelength (nm)	Term	Observed peak wavelength (nm)	Integrated wavelength interval (nm)	Cross section at 200 eV (10^{-19} cm^2)	Cross section at 100 eV (10^{-19} cm^2)	Other measurements at 200 eV (100 eV) (10^{-19} cm^2)
	N II	91.5962	$g\,^3P$–$^3P^\circ$					
	N II	91.6012	$g\,^3P$–$^3P^\circ$					
	N II	91.6020	$g\,^3P$–$^3P^\circ$					
	N_2	91.6422	b(11,0)					
	N II	91.6701	$g\,^3P$–$^3P^\circ$					
	N II	91.6710	$g\,^3P$–$^3P^\circ$					
B	N_2	91.789	c_5'(0,3)	91.81	91.74–91.91		0.49	
	N_2	91.820	b'(14,2)					
C	N_2	92.314	$c_4'(3,1)^+$	92.32	92.28–92.40		0.56	
	N_2	92.356	b_4'(13,2)					
D	N_2	92.476	$c_4'(4,2)^+$	92.49	92.44–92.49		0.10	
22				92.9	92.6–93.6	3.1	2.51	
A	N_2	92.707	b'(9,1)	92.74	92.68–92.83		1.42	
	N_2	92.72	b'(16,3)*					
B	N_2	92.886	$c_4'(6,4)^+$	92.87	92.83–93.28		0.90	
	N_2	92.892	b(9,0)					
	N_2	93.1735	b'(15,0)					
C	N_2	93.271	b'(8,1)	93.31	93.28–93.38		0.19	
23				94.4	93.6–95.1	7.4	9.42	
A	N_2	93.789	b'(7,1)	93.87	93.83–93.95		0.47	
	N_2	93.856	c_3(1,0)					
B	N_2	94.0128	c_4'(1,0)	94.03	93.98–94.07		0.14	
	N_2	94.015	c_3(2,1)					
	N_2	94.064	b'(10,2)*					
C	N_2	94.1449	c_4'(2,1)	94.24	94.22–94.27		0.27	
	N_2	94.2413	b(7,0)					
D	N_2	94.317	$c_4'(3,2)^+$	94.31	94.27–94.39		2.04	
		94.336	b'(13,3)					
E	N_2	94.4562	b'(3,0)	94.46	94.39–94.62		3.46	
	N_2	94.460	$c_4'(4,3)^+$					
F	N_2	94.691	$b'(16,4)^+$	94.73	94.67–94.78		1.09	
	N_2	94.728	b'(9,2)					
G	N_2	94.837	$c_4'(6,5)^+$	94.83	94.78–94.92		1.95	
	N_2	94.9249	b(6,0)					
24				95.8	95.1–97.6	69.7	88.0	
A	N I	95.230 37 ST	$g\,^4S^\circ$–^4D	95.24	95.17–95.28		0.94	
	N I	95.241 51 ST	$g\,^4S^\circ$–^4D					
	N_2	95.242	b'(5,1)					
	N I	95.252 31 ST	$g\,^4S^\circ$–^4D					
B	N_2	95.317	b'(8,2)	95.41	95.28–95.44		3.84	
	N I	95.341 50	$g\,^4S^\circ$–^4P					
	N I	95.365 48	$g\,^4S^\circ$–^4P					
	N_2	95.380	b'(18,5)					
	N I	95.396 98	$g\,^4S^\circ$–^4P					
	N I	95.410 40	$g\,^4S^\circ$–^4F					
C	N_2	95.5108	b(5,0)	95.84	95.44–96.08		74.7	31.1[a]
	N_2	95.532	b'(11,3)					68.1[c]
	N_2	95.706	c_5'(0,3)					87.8[f]
	N_2	95.7683	b'(1,0)					60[g]
	N_2	95.792	b'(14,4)*					

TABLE I. (*Continued*).

Feature No.	Species	Wavelength (nm)	Term	Observed peak wavelength (nm)	Integrated wavelength interval (nm)	Cross section at 200 eV (10^{-19} cm^2)	Cross section at 100 eV (10^{-19} cm^2)	Other measurements at 200 eV (100 eV) (10^{-19} cm^2)
	N_2	95.8565	$c_4'(0,0)$*					
	N_2	95.858	$b'(7,2)$					
	N I	95.949 36	$g\ ^4S°–^2P$					
	N_2	95.970	$c_3(1,1)$					
	N I	96.020 17	$g\ ^4S°–^2P$					
D	N_2	96.094	$c_3(2,2)$	96.12	96.08–96.15		0.70	
	N_2	96.118	$c_4'(1,1)$					
	N_2	96.148	$b'(17,5)$					
E	N_2	96.234	$c_4'(2,2)$	96.16	96.15–96.31		0.30	
F	N_2	96.357	$b(7,1)$	96.40	96.31–96.43		3.04	
		96.383	$c_4'(3,3)^+$					
	N I	96.399 04 ST	$g\ ^3S°–^4P$					
G	N_2	96.4564	$b'(0,0)$	96.47	96.43–96.57		3.22	
	N I	96.462 58 ST	$g\ ^4S°–^4P$					
	N I	96.504 15 ST	$g\ ^4S°–^4P$					
	N_2	96.506	$c_4'(4,4)^+$					
	N_2	96.5728	$b(4,0)$					
H	N_2	96.742	$b'(6,2)$	96.82	96.70–96.94		0.86	
	N_2	96.812	$b'(9,3)$					
	N_2	96.845	$c_4'(6,6)^+$					
I	N_2	96.962	$b'(19,6)^+$	97.03	96.96–97.05		0.35	
	N_2	97.002	$b'(12,4)$*					
25				98.1	97.6–100.1	19.8	21.0	4.1[a] 7.29[c] 22.9[f]
A	N_2	98.046	$c_4'(0,1)$*	98.04,0.08	97.97–98.17		12.29	
B	N_2	98.237	$b'(10,4)$	98.30	98.22–98.42		0.76	
	N_2	98.295	$c_4'(1,2)$					
	N_2	98.385	$c_4'(2,3)$					
C	N_2	98.514	$c_4'(3,4)^+$	98.52	98.48–98.54		1.21	
D	N_2	98.542	$b(7,2)$	98.63	98.54–98.75		4.09	
	N_2	98.5691	$b(1,0)$*					
	N_2	98.614	$c_4'(4,5)^+$					
E	N_2	98.795	$b(4,1)$	98.81	98.75–98.85		0.25	
	N_2	98.809	$b'(16,6)$					
F	N_2	98.911	$c_4'(6,7)^+$	98.90	98.85–98.94		1.27	
	N_2	98.917	$b'(6,3)$					
G	N_2	98.962	$b'(9,4)$	98.95	98.94–99.13		0.96	
	N_2	99.033	$b'(19,7)$					
H	N_2	99.132	$b'(12,5)$	99.16	99.11–99.19		0.21	
	N_2	99.1897	$b(0,0)$					
26				100.9	100.1–102.1	6.9	5.8	
A	N_2	100.310	$c_4'(0,2)$	100.29	100.24–100.40		1.21	
	N_2	100.376	$c_3(1,3)$					
B	N_2	100.538	$c_4'(1,3)$	100.57	100.52–100.61		0.20	
	N_2	100.607	$c_4'(2,4)^+$					
C	N_2	100.711	$c_4'(3,5)^+$	100.71	100.69–100.85		1.05	
	N_2	100.787	$c_4'(4,6)^+$					
D	N_2	100.885	$b(1,1)$*	100.91	100.85–100.94		1.18	
E	N_2	100.961	$b'(16,7)$	100.98	100.94–101.03		1.03	

TABLE I. (*Continued*).

Feature No.	Species	Wavelength (nm)	Term	Observed peak wavelength (nm)	Integrated wavelength interval (nm)	Cross section at 200 eV (10^{-19} cm^2)	Cross section at 100 eV (10^{-19} cm^2)	Other measurements at 200 eV (100 eV) (10^{-19} cm^2)
F	N_2	101.039	$c'_4(6,8)^+$	101.05	101.03–101.11		0.57	
G	N_2	101.180	$b'(9,5)$	101.24	101.17–101.28		0.51	
	N_2	101.234	$o_3(0,3)$					
H	N_2	101.581	$b(6,3)$	101.58	101.57–101.63		0.09	
38	N I	119.954 90 ST	$g\,^4S°–^4P$	120.0	119.3–121.1	31.1	40.0	35[b]
	N I	120.022 38 ST	$g\,^4S°–^4P$					31.7[d]
	N I	120.071 13 ST	$g\,^4S°–^4P$					31.0[e]
								(40.0)[e]

[a]Morgan and Mentall, Ref. 19; cross section corrected as indicated in text by factor of 0.607.
[b]Aarts and de Heer, Ref. 20; measurement interval not known.
[c]Zipf and McLaughlin, Ref. 18.
[d]Mumma and Zipf, Ref. 31; cross section corrected as indicated in text by factor of 0.619.
[e]Ajello and Shemansky, Ref. 35; measurement corrected by 0.892 as indicated in text.
[f]McLaughlin, Ref. 49; corrected as indicated in text by 0.619.
[g]J C. Huschilt, Dassen, and McConkey; Ref. 20.

Ar I, Ar II multiplets are used as calibration sources, in addition to the double monochromator technique.[36]

One additional calibration procedure must be considered. The absolute cross section of *N* I (119.99 nm) used to normalize the entire vuv spectrum is determined by the relative flow technique developed at the Jet Propulsion Laboratory.[25,45] In this method the Lyman-α fluorescence signal at 100-eV impact energy from H_2, the standard gas, is compared to the fluorescence signal from N I (119.99 nm) emission produced by electron impact at 100 eV on N_2, the unknown gas, at low background pressures in the molecular flow gas regime. The comparisons are made over a range of background gas pressures from 3×10^{-7} to 1×10^{-5} to establish linearity of signal with pressure. For comparison of the signal strengths in the linear region, a value of 7.3×10^{-18} cm^2 was used as the cross section[27] for Lyman-α production by dissociative excitation of H_2 at 100 eV. By this method the cross section for N I (119.99 nm) at 100 eV was measured by Ajello and Shemansky[35] to be 4.48×10^{-18} cm^2. However, the value of the H_2 Lyman-α cross section used in this previous measurement[26] was 8.18×10^{-18} cm^2. The revised H_2 Lyman-α cross section of Pang *et al.*[27] yields a revised N I (119.99 nm) cross section of 4.0×10^{-18} cm^2 at 100 eV. Reference 35 shows that the agreement among the various experimental groups for the N I (119.99 nm) multiplet is better than 18% with the revised Lyman-α cross section. The absolute cross section for the dominant N_2 $c'_4\,^1\Sigma_u^+(0,0)$ band at 95.84 nm (feature 24C in Table I) was then measured with reference to N I (119.99 nm) by the relative flow technique to be 7.47×10^{-18} cm^2 at 100 eV. The root sum square uncertainty for the absolute cross sections given in this work is estimated to be 22%, based on the uncertainties in the corrected Lyman-α cross section,[27,36] relative calibration, and signal statistics.

The background gas pressure for the present determination of N_2 emission cross sections must be carefully chosen to ensure optically thin conditions and to avoid self-absorption effects, particularly for the $c'_4\,^1\Sigma_u^+(0,0)$ resonance band at 95.8 nm. The operating pressure must result in an optical depth at the line center of less than 0.1 for the optical path length involved. Below this presure the measured cross section will be independent of pressure. Two approaches have been used to determine the maximum background gas pressure that can be used and still maintain optically thin conditions.

The relative intensities of the $c'_4\,^1\Sigma_u^+(0,0)$ band at 95.8 nm, N II $g\,^3P–^3P°$ multiplet at 91.60 and 91.67 nm, and the $c'_4\,^1\Sigma_u^+(0,1)$ band at 98.0 nm have been measured as a function of pressure over the range 4×10^{-7} to 3×10^{-5} Torr. The N II line is not expected to exhibit any optical depth effects in this pressure range and acts as a normalization feature. The experimental intensity ratios of these features are shown in Fig. 3. The intensity ratios for both (95.8 nm)/(91.6 nm) and (95.8 nm)/(98.0 nm) are approximately constant up to a background gas pressure of 6×10^{-6} Torr when they begin to decrease, indicating the effect of self-absorption at 95.8 nm. It is interesting to note the invariance of the intensity ratio (98.0 nm)/(91.6 nm) with pressure, which suggests that the energy from self-absorption at 95.8 nm is not solely directed into the $c'_4\,^1\Sigma_u^+(0,1)$ transition at 98.0 nm. A theoretical model has also been developed to predict the variation of these intensity ratios with pressure and is also shown in Fig. 3. The attenuation or relative absorption (I/I_0) experienced by radiation passing through a slab of absorbing molecular gas is given by Beer's law

$$\frac{I}{I_0}=e^{-n\sigma_{v'0}l}=e^{-\tau},$$

where n is the number density of the absorbing gas, $\sigma_{v'0}$ is the absorption cross section over the Doppler width ($\Delta\nu_D$) of the rotational line for the vibrational transition ($v',0$) l is the optical path length, and τ is the optical depth at line center. The model for the $c_4'\,{}^1\Sigma_u^+(0,0)$ transition shown in Fig. 3 is for an individual rotational transition from $J''=7$, the peak in the thermal distribution at 300 K. The absorption cross section at line center is obtained using the optical oscillator strength ($f_{0v'}$) for the $c_4'(0,0)$ transition[23] and the Doppler width ($\Delta\nu_D$). The cross section is weighted by the Honl-London factor $S_{J'J''}/(2J''+1)$ for the R branch. It is given by

$$\sigma_{v'0}=\frac{\pi e^2}{mc}f_{0v'}\left[\frac{S_{J'J''}}{2J''+1}\right]\frac{1}{\sqrt{\pi}\Delta\nu_D}\ . \tag{1}$$

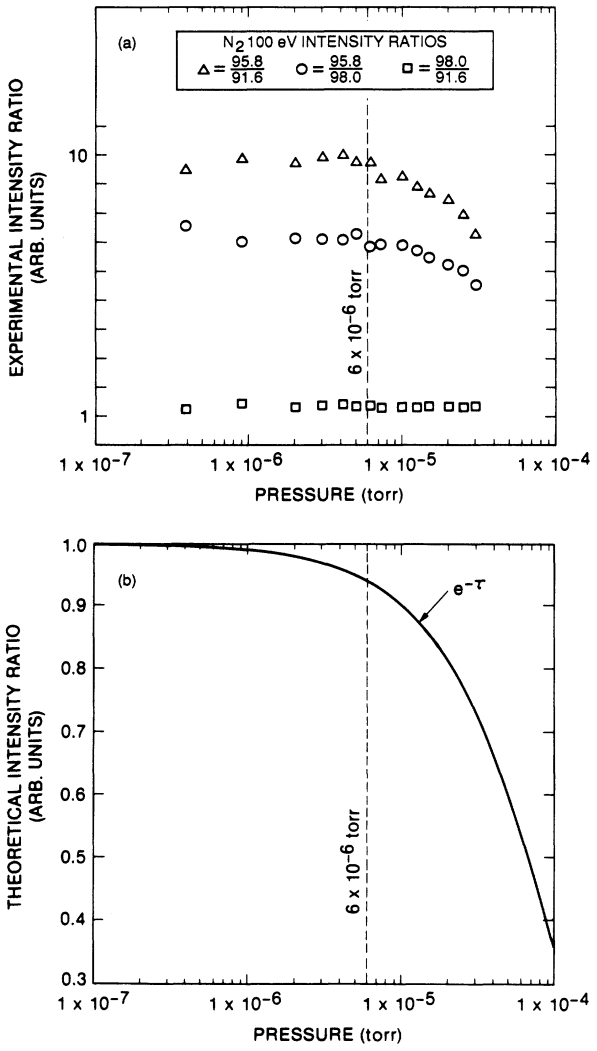

FIG. 3. Linearity test for cross-section measurements vs gas background pressure in the chamber for the N_2 $c_4'(0,0)$ resonance band at 95.8 nm. (a) The $c_4'(0,0)$ band signal was compared as a function of pressure to the N II (91.6-nm) multiplet signal and the $c_4'(0,1)$ band signal at 98.0 nm. Also, the $c_4'(0,1)$ band was compared as a function of pressure to the N II (91.6-nm) signal. (b) Theoretical curve for the intensity ratio of $c_4'(0,0)$ band to an optically thin line.

The theoretical plot of $e^{-\tau}$ against pressure shown in Fig. 3 supports the experimental determination. At a background pressure of 6×10^{-6} Torr the calculated optical depth at line center for 95.8 nm is 0.06. For rotational transitions from levels other than $J''=7$ the optical depths are even smaller.

EXPERIMENTAL RESULTS: LOW-RESOLUTION RESULTS 40–120 nm

The low-resolution electron-impact spectrum of N_2 at 200 eV is shown in Figs. 4 and 5. This spectrum is an optically thin, calibrated spectrum of N_2 at a resolution of 0.5 nm at a gas background pressure of 2.5×10^{-6} Torr.

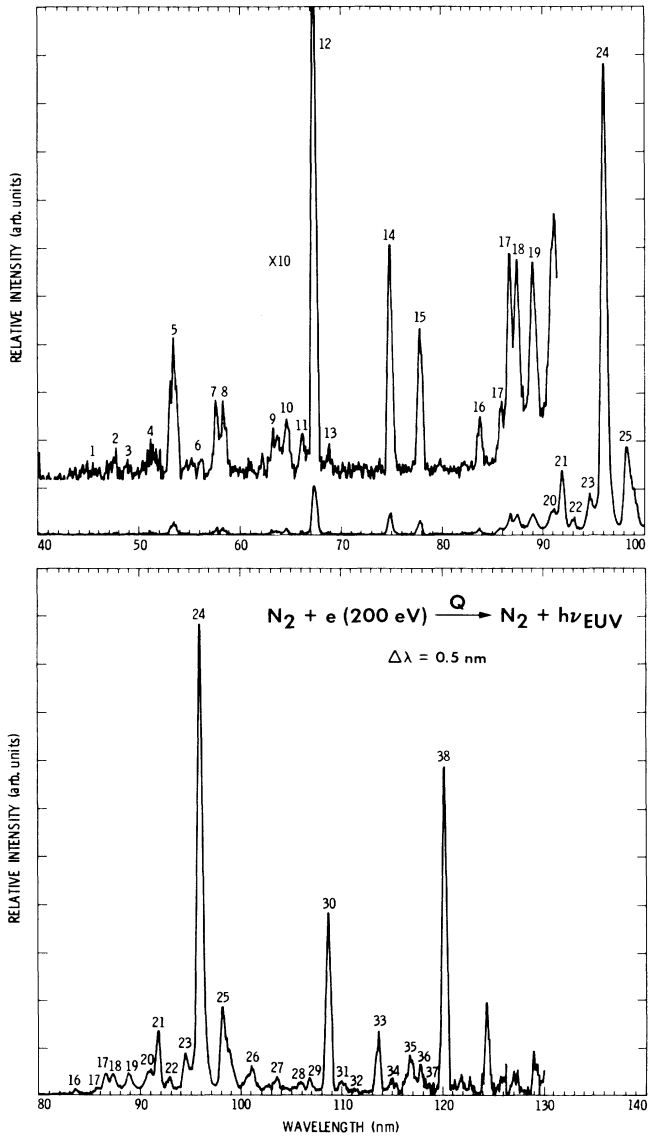

FIG. 4. Calibrated spectrum of N_2 at 200-eV electron-impact energy at 0.5-nm resolution from 40 to 130 nm. The spectrum was obtained in the crossed-beam mode at 2.5×10^{-6}-Torr background gas pressure. The feature numbers are listed in Table I with identifications and cross sections.

The features in Fig. 4 are identified by feature numbers that increase from 1 to 38. The last feature is the 120.0-nm resonance line of N I that starts the fuv region. Features in the fuv have been identified in a previous paper by Ajello and Shemanksy.[35] Features 1–26 are discussed in this paper and features 27–38 will be treated in Ref. 3. Table I lists the candidate identifications of the contents of each feature, many of which are combined blends of atomic multiplets and molecular transitions at this resolution. The identifications of the N I and N II multiplets are taken from Ref. 46. The N_2 band origins are from Roncin, Launay, and Yoshino[17] for $v''\neq 0$; the band origins for the bands of the $b'\,^1\Sigma_u^+ \rightarrow X\,^1\Sigma_g^+(0)$ transitions are from Carroll, Collins, and Yoshino;[5] and the band origins for the $c_4'\,^1\Sigma_u^+ \rightarrow X\,^1\Sigma_g^+(0)$ transisitions are from Yoshino and co-workers[6,7] ($v'=0$–4) and Carroll, Collins, and Yoshino[5] ($v'=5,6$). The $b\,^1\Pi_u$ ($v>7$) $\rightarrow X\,^1\Sigma_g^+$ bands have never been observed in emission but are included as candidate wavelengths for completeness. Accurate band origins can be also found in Stahel, Leoni, and Dressler[10] for the b', c_4', and b band systems. Table I lists the cross section at 200 eV for each feature.

The features in Fig. 5 are identified by N I and N II Rydberg series. The identification of features as combined N I, N II or/and N III multiplets in Fig. 5 is unambiguous below 80 nm; there are no observed N_2 or N_2^+ transitions at wavelengths less than the energy of the first ionization potential. For wavelengths above 80 nm, the higher-resolution work of the subsequent sections is needed to show that the N I multiplet cross sections are very small compared to nearby molecular features. In general, the first member of the Rydberg series is the strongest feature by one or two orders of magnitude compared to the next member. For example, the cross section of the N I (120.0 nm) multiplet with principal quantum number $n=3$ is 40.0×10^{-19} cm^2 at 100 eV, while the cross section of the N I (96.5 nm) multiplet $n=4$ is about 1×10^{-19} cm^2.

Below 80 nm the strongest feature, No. 12, is the N II multiplet at 67.1 nm. The excitation function of this feature is shown in Fig. 6. The cross section peaks at 170 eV with a cross-section value of 6.8×10^{-20} cm^2. The N II multiplets at 91.6 and 108.5 nm, features 21 and 38, respectively, are also very strong. The 108.5-nm feature is discussed in Ref. 3.

MODEL

The Rydberg and valence states of N_2 that are important for understanding the euv emission spectra are shown in the partial energy-level diagram in Fig. 7. The $b'\,^1\Sigma_u^+$ and $b\,^1\Pi_u$ states are classified as valence states, and the $c_n\,^1\Pi_u$, $c_n'\,^1\Sigma_u^+$, and $o_n\,^1\Pi_u$ states are classified as Rydberg states according to the way the states dissociate into unexcited ($^4S^0, ^2D^0, ^2P^0$) or excited N atoms outside of the ground configuration, respectively. The right-hand

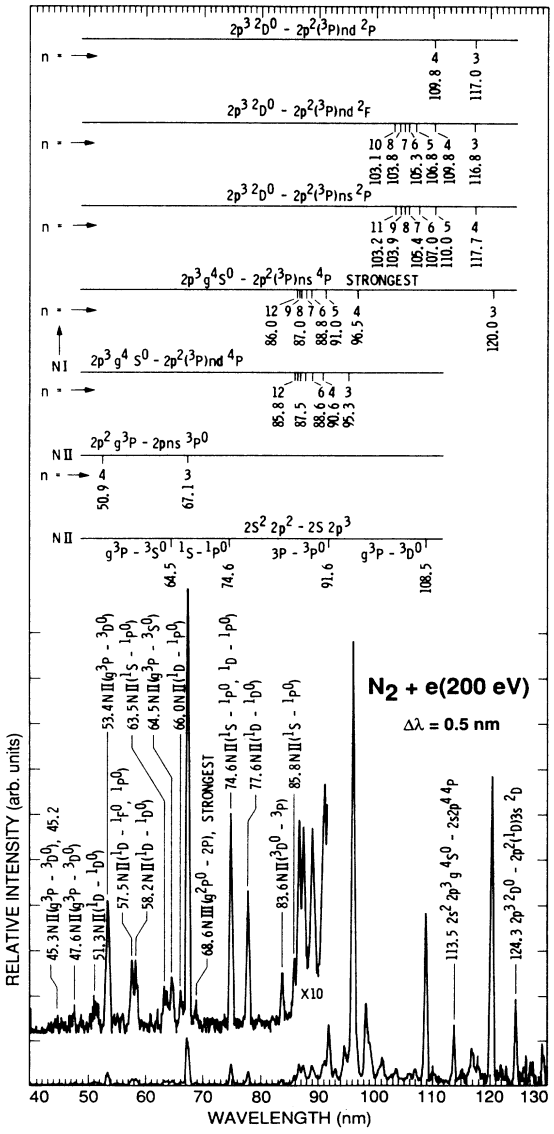

FIG. 5. Calibrated spectrum of N_2 at 200 eV as in Fig. 4. Many of the features are identified by Rydberg series.

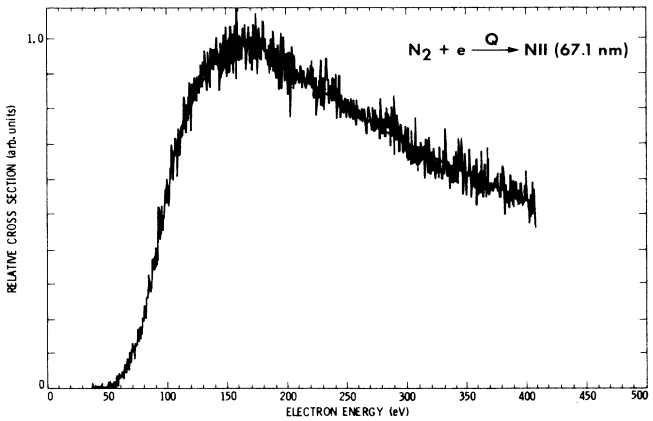

FIG. 6. Relative emission cross section of the N II (67.1-nm) multiplet from dissociative ionization of N_2.

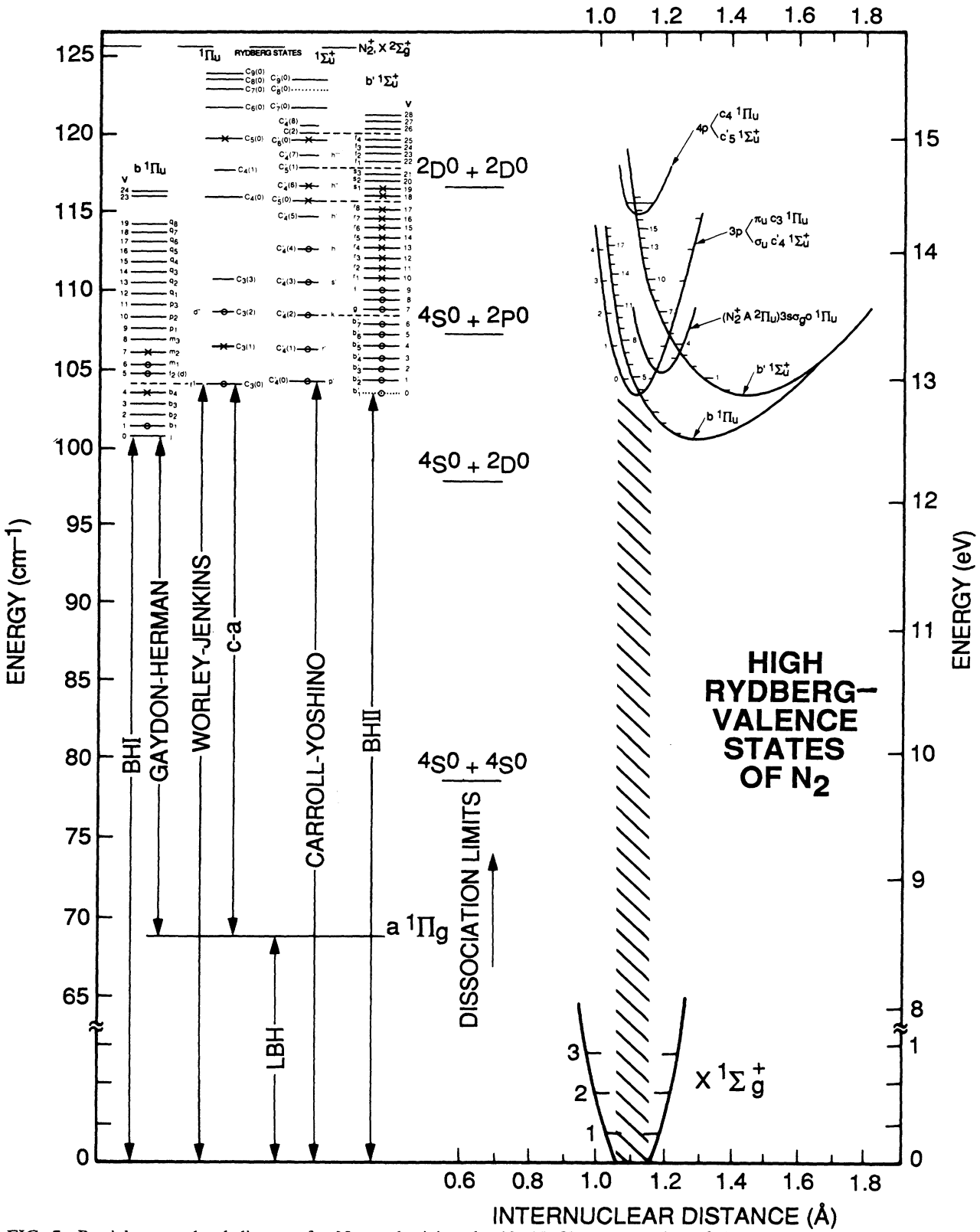

FIG. 7. Partial energy-level diagram for N_2 emphasizing the 12–15-eV energy region of the Rydberg and valence states. The right-hand side of the figure shows the diabatic potential curves from Dressler (Ref. 13) and the left-hand side observed vibrational levels from Carroll and Collins (Ref. 4). The circles indicate levels observed in emission with single circle representing those observations prior to work of Lofthus and Krupenie (Ref. 12) and ×'s those observed in Roncin, Launay, and Yoshino (Ref. 17) or in this work.

side of Fig. 7 shows the unperturbed diabatic potential curves of the states from Dressler.[13] The left-hand side of Fig. 7 from Carroll and Collins[4] shows the perturbed energy levels of the same states. Note the irregular spacing of vibrational intervals. Small circles are used to indicate levels that have been seen in emission previous to the work of Lofthus and Krupenie[12] (single circles) and by Roncin, Launay, and Yoshino[17] or this work (x's). In absorption the b', up to $v'=28$, and c' series, up to $v'=7$, are sharp except for diffuseness in the spectra of $v'=20,21,22$ of the b' series.[5]

In emission a rich band system for each of the b' and c' states is expected. A synthetic spectrum based on the diabatic potential curves and perturbed energy levels given in Carroll, Collins, and Yoshino[5] is shown in Fig. 8. The relative intensity[36] band is given by

$$I_{v'v''}=Q_{v'}\omega_{v'v''}/Q \ , \tag{2}$$

where

$$\omega_{v'v''}=A_{v'v''}/A_{v'} \ . \tag{3}$$

In the Born limit we write

$$Q_{v'} \propto A_{v'}\lambda^3_{v'0} \tag{4}$$

and

$$\mu^2_{v'0} \propto A_{v'0}\lambda^3_{v'0} \ , \tag{5}$$

where $Q_{v'}$ and Q are excitation cross sections to level v' and all levels, respectively, $\mu_{v'0}$ is the dipole transition moment, $A_{v'v''}$ is the emission transition probability, $A_{v'}$ is the total transition probability (emission plus predissociation), and $\omega_{v'v''}$ is the emission branching ratio. For the unperturbed case where the electronic transition moment is assumed constant, we calculate Franck-Condon factors $q_{v'0}$, using a Morse potential. The c'_4 band system shown in the top portion of Fig. 8 is expected to have a strong (0,0) band containing 97% of the band-system intensity with an R-branch head[47] at 95.8170 nm and a P-branch[7] origin at 95.8562 nm. Our spectra at 0.03-nm resolution resolve these two branches. The potential curves of the c'_4 and X electronic states have nearly identical equilibrium internuclear distances. The (0,1) band at 98.05 nm and the (1,1) band at 96.07 nm are also expected to have measurable intensity. Other bands from higher levels ($v'>1$) are expected to produce negligible intensity.

On the other hand, the b' band system with an equilibrium distance of 1.44 A is shown to be spread out in wavelength from 85 to 105 nm. The $v''=0$ progression from 85 to 92 nm is the strongest progression and the (16,0) band at 87.14 nm the strongest band within the progression. For this reason the region 92–102 nm was chosen for higher-resolution work on the c'_4 state, and 82–92 nm for the b' state.

In general, each of the levels of the b' and c'_4 series indicated in Fig. 7 is perturbed most strongly by the level of the other series that is most nearly in energy resonance with it. For the perturbed case of coupling of electronic-nuclear motion between two vibrational levels (1,2) such as the vibrational levels of the b' and c'_4 states, above, we show that we can calculate the resultant intensity as a sum of borrowing and interference intensities. The resultant mixed eigenstates (+, −) produce a vibrational band of mixed character whose intensity is given by an expression similar to (2) above. For example, for the higher-energy (+) state

$$I_{v^+,v''} \propto A_{v^+,0}\lambda^3_{v'0}\omega_{v^+,v''} \ , \tag{6}$$

$$\mu^2_{v^+,0} \propto A_{v^+,0}\lambda^3_{v',0} \ , \tag{7}$$

$$\mu_{v^+,0}=c_1\mu_{10}+c_2\mu_{20} \ , \tag{8}$$

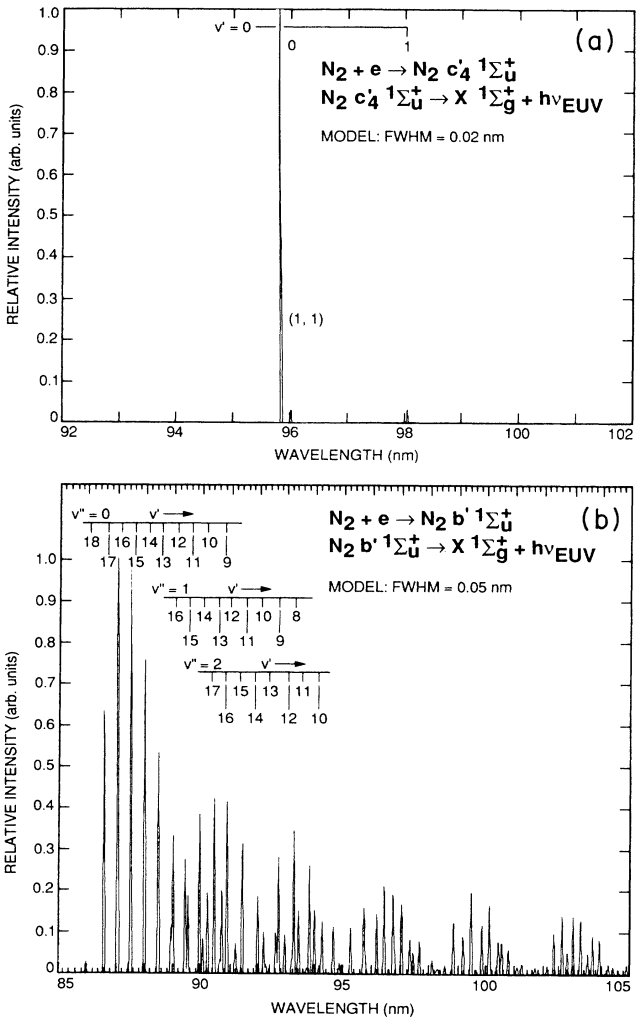

FIG. 8. (a) Synthetic direct excitation spectrum of $c'_4\ ^1\Sigma_u^+ \rightarrow X\ ^1\Sigma_g^+$ bands based on diabatic potential curves in Fig. 7 without rotational structure. The molecular constants are taken from Huber and Herzberg (Ref. 11). The synthetic spectrum is convolved with a 0.02-nm triangular instrumental band pass. (b) Synthetic direct excitation spectrum of $b'\ ^1\Sigma_u^+ \rightarrow X\ ^1\Sigma_g^+$ bands with a 0.05-nm band pass. The band heads for the $(v',0)$ transition are from Lofthus and Krupenie (Ref. 12). The band origins from the nonresonance transitions are from Roncin, Launay, and Yoshino (Ref. 17). The calculated band origins are not sufficiently accurate using molecular constants of Huber and Herzberg (Ref. 11) to compare to the data for high v'.

and

$$\mu^2_{v^+,0}=c^2_{1+}\mu^2_{10}+c^2_{2+}\mu^2_{20}+2c_{1+}c_{2+}\mu_{10}\mu_{20}\ , \qquad (9)$$

where c_{1+} and c_{2+} are eigenvector components, which have been tabulated by Stahel, Leoni, and Dressler,[10] The first two terms in Eq. (9) are the borrowing terms and the third term is the interference term. If $c_{2+}=0$ and $c_{1+}=1$, the intensity is the same as the deperturbed case above. A similar term can be derived for the emission branching ratio involving the (+) level with each of the ground-state vibrational levels (v'').

For example, in Fig. 7 the c'_4 ($v'=0$) level is perturbed most strongly by the b' ($v'=1$) level. The b'-c'_4 interaction increases from a weak interaction between b' ($v'=1$) and c'_4 ($v=0$), discussed above, to a maximum amplitude between levels b' ($v'=7$) and c'_4 ($v'=2$) and decreasing in amplitude afterward for both states for larger v. For high v' (~ 18) the c'_5 (also known as the e' state) replaces the c'_4 as the perturbing state. A quantitative analysis of the b'-c'_4 electron-impact excitation spectrum of Geiger and Schroder on the basis of the vibronic interaction matrix is given by Stahel, Leoni, and Dressler.[10]

OVERVIEW TO MEDIUM-RESOLUTION SPECTRUM 92–102 nm

We show in Figs. 9 and 10 the medium-resolution spectra at 0.03-nm resolution of N_2 at 100 and 20 eV, respectively, from 92 to 102 nm. The spectral features are identified by feature number as in Fig. 4 and are further subdivided according to a letter starting with A for the shortest wavelength feature in the interval. The transitions within each c'_4 progression that are observed in our experiment are indicated in the figures. The cross sections at 100 eV for each of these vibronic features from Figs. 9 and 10 are given in Table I for each feature from $21C$ to $26D$, along with candidate identifications that may overlap them. A detailed analysis at 100 and 20 eV of the features containing c'_4 bands is given in Table II, eliminating many of these candidate features as strong contributors (> 10% of the emission intensity). Table II also includes higher-energy vibronic features from the euv spectra from 83 to 92 nm shown in Figs. 12 and 13 to be discussed in the next section. The following criteria were useful in many cases in eliminating candidate features: (1) N I lines are only present in 100-eV spectra, (2) mea-

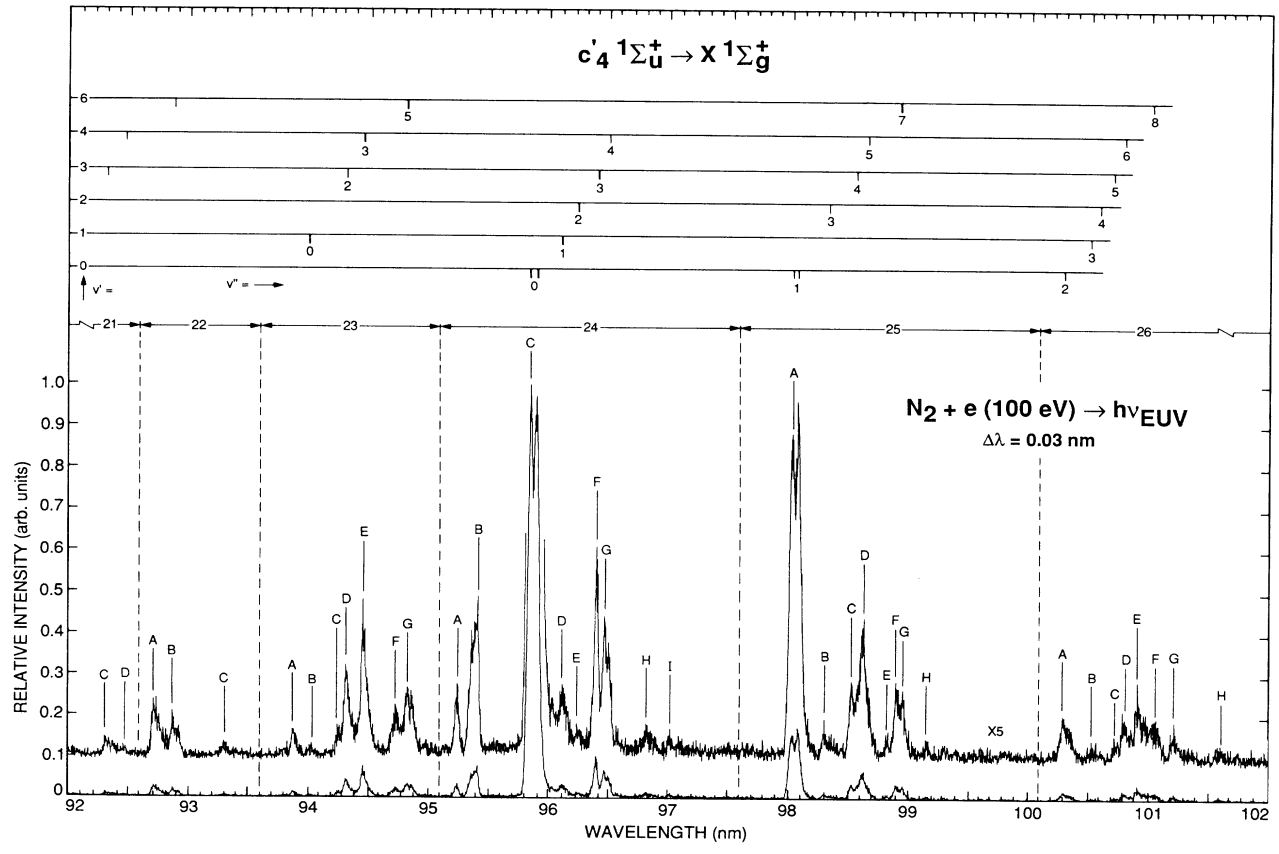

FIG. 9. Calibrated, optically thin high-resolution spectrum of N_2 from 92 to 102 nm produced by electron impact at 100 eV. The resolution was 0.03 nm. Feature numbers and letters can be found in Table I. The vibrational progressions for $v'=0,1,2,3,4,6$ are indicated for the $c'_4\ ^1\Sigma_u^+ \rightarrow X\ ^1\Sigma_g^+$ Carroll-Yoshino band system. The background gas pressure was 6×10^{-6} Torr.

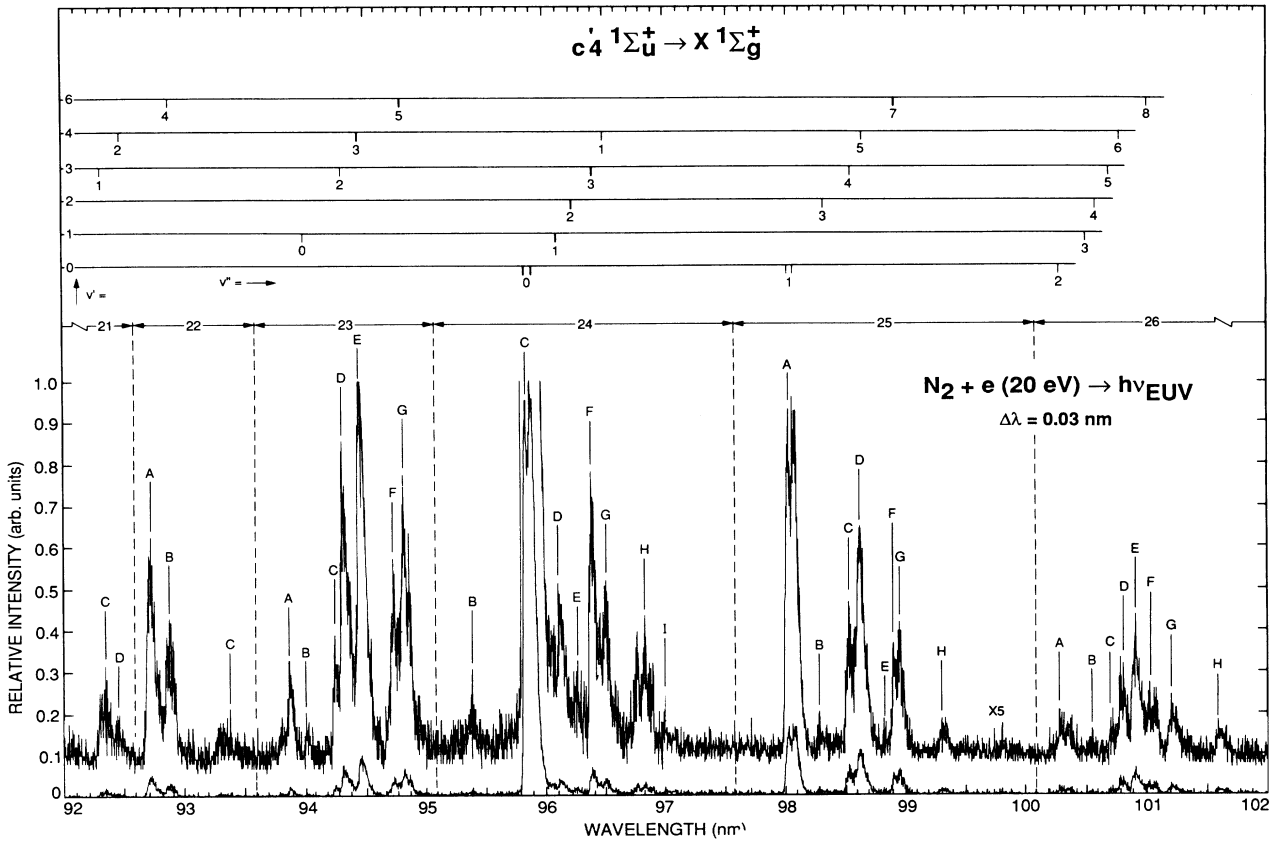

FIG. 10. Same as Fig. 9 for electron impact at 20 eV.

TABLE II. Vibrational analysis of $c'_4\,{}^1\Sigma_u^+ \rightarrow X\,{}^1\Sigma_g^+$ bands at 20 and 100 eV electron-impact energy.

v'	v''	λ (nm) band origin[a]	Feature No.	Principal overlap features[d]	Experimental: Absolute Q (10^{-19} cm^2)	100 eV Relative Q	Experimetal: Absolute Q (10^{-19} cm^{-2})	20 eV Relative Q	Relative Q direct theory	Direct $q_{v'0}$ Franck-Condon factor	Experimental Franck-Condon factor: this work at 100 eV vs energy loss[c]
0	0	95.8565	24*C*	*b*′(7,2)	74.7	1.00	20.6	1.00	1.00		
	1	98.046	25*A*		12.3	0.165	3.39	0.165	0.0309		
	2	100.310	26*A*		1.21	0.0162	0.31	0.015	0.000 761		
	3	102.649	27*B*		0.52	0.0070	0.07	0.0093	0.000 051		
	4	105.069	27*L*		0.22	0.0029	0.08	0.0039			
	5	107.573	30*A*	$c'_4(2,7)$, $c'_4(1,6)$	~0.10	~0.0013	~0.03	0.0015			
	Total				$Q_{v'=0}=88.8$		$Q_{v'=0}=24.6$			0.967	0.73(0.78)
1	0	94.013	23*B*		<0.14		<0.03				
	1	96.118	24*D*		~0.70		~0.24				
	2	98.295	25*B*	$c'_4(2,3)$	~0.66		~0.22				
	3	100.538	26*B*	$c'_4(2,4)$	~0.10		~0.03				
	4	102.859	27*C*	$c'_4(2,5)$ N I lines	~0.						
	5	105.257	28*A*	N I lines	~0.09						
	6	107.736	30*A*	$c'_4(2,7)$	~0.5						
	Total				$Q_{v'=1}\simeq 2.1$		$Q_{v'=1}\simeq 0.7$			0.032	~0.017(0.007)

TABLE II. (*Continued*).

v'	v''	λ (nm) band origin[a]	Feature No.	Principal overlap features[d]	Experimental: Absolute Q (10^{-19} cm^2)	100 eV Relative Q	Experimental: Absolute Q (10^{-19} cm^2)	20 eV Relative Q	Relative Q direct theory	Direct $q_{v'0}$ Franck-Condon factor	Experimental Franck-Condon factor: this work at 100 eV vs energy loss[c]
2	0	92.128			~0.0		~0				
	1	94.149	23*C*		0.27		0.09				
	2	96.234	24*E*		0.30		0.14				
	3	98.385	25*B*	$c_4'(1,2)$	~0.1		~0				
	4	100.607	26*B*	$c_4'(1,3)$	~0.1		~0.03				
	5	102.900	27*C*	$c_4'(1,3)$, N I lines	~0.0		~0				
	6	105.268	28*B*	$c_4'(3,7)$, N I lines	~0.14		~0.04				
	7	107.714	30*A*	$c_4'(0,5)$, $c_4'(1,6)$	~0.5		~0.16				
	Total				$Q_{v'=2} \simeq 1.4$		$Q_{v'=1} \simeq 0.5$			5.0×10^{-4}	~0.011(~0.0)
3	0	90.370	20*B*	$b'(13,1)$	0.40		~0.19				
	1	92.314	21*C*	$b'(13,2)$	0.44		~0.24				
	2	94.317	23*D*		~2.04		~1.07				
	3	96.383	24*F*	N I line, $b(7,1)$	2.2		1.06				
	4	98.516	25*C*		1.21		~0.61				
	5	100.711	26*C*	$c_4'(4,6)$	~0.5		~0.1				
	6	102.979	27*C*	$c_4'(1,3)(2,5)$, N I lines	~0.		~0.				
	7	105.318	28*B*	$c_4'(2,6)$, N I lines	~0.14		~0.04				
	Total				$Q_{v'=3} \simeq 6.9$		$Q_{v'=4} \simeq 3.3$			2.1×10^{-6}	0.057(0.05)
4	0	88.678	19*C*	N I lines, $b'13,0$	~2.5		0.97				
	1	90.549	20*C*	N I lines	~1.5		0.49				
	2	92.476	21*D*		0.10		0.03				
	3	94.460	23*E*		3.47		1.36				
	4	96.506	24*G*	N I lines	~3.0		1.0				
	5	98.614	25*D*	$b(1,0)$	~2.9		~1.1				
	6	100.787	26*C*	$c_4'(3,5)$	~0.1		~0.1				
	7	103.027	27*D*	$b(7,4)$, N I lines	~0.		~0.				
	8	105.337	28*B*	$c_4'(2,6)(3,7)$, N I lines	~0.		~0.				
	Total				$Q_{v'=4} \simeq 14.0$		$Q_{v'=4} \simeq 5.1$			6×10^{-6}	0.12(0.13)
6	0	85.612	17*C*	$b'(19,0)$	0.73		~0.29				
	1	87.354	18*B*		0.89		0.30				
	2	89.146	19*D*	$b'(12,0)$	<1.27		<0.65				
	3	90.989	20*E*	$b'(12,1)$, N I lines	<1.69		<0.48				
	4	92.886	22*B*		0.90		0.38				
	5	94.837	23*G*		1.95		0.92				
	6	96.845	24*H*	$b'(9,3)$, $b'(6,2)$	<0.86		<0.36				
	7	98.911	25*F*		1.27		0.61				
	8	101.039	26*F*		0.57		~0.23				
	9	103.229	27*E*	$b(1,2)$, N I lines	~0.		~0.				
	total				$6.3 < Q_{v'=6} < 10.1$		$2.7 < Q_{v'=6} < 4.2$			$<10^{-7}$	0.052–0.083(0.04)
	Grand total				$Q_{v'=6} \simeq 8.2$ $Q = 121.4$[b]		$Q_{v'=6} \simeq 3.45$ $Q = 37.7$[b]				

[a]Band origin wavelengths from Roncin, Launay, and Yoshino, Ref. 17 and Yoshino and Tanaka, Ref. 7.

[b]Man value of Q in units of 10^{-19} cm^2.

[c]Experimental Franck-Condon factors $q_{v'0}$. This work is first entry. Geiger and Schroder, Ref. 2 energy loss data for $v'=0,1,2,3,4,6$ is second entry in parentheses.

[d]See Roncin, Launay, and Yoshino, Ref. 17 for strong overlap features that lie within 0.05 nm of measured peak wavelength. There are exceptions for $c_4'(4,6)$ and $c_4'(3,5)$ unresolved and $c_4'(1,2)$ and $c_4'(2,3)$ unresolved.

sured thermal-energy emission peaks ($J_{max} \sim 7$) lie within 0.05 nm of the published band origins, (3) weak or very weak discharge lamp bands correlate to weak electron-impact bands except for resonance transitions, (4) we apply the model and analysis of Stahel, Leoni, and Dressler to separate blended resonance bands of b' and c_4' systems. After applying these criteria the cross sections for most bands are determined to an experimental accuracy of 22%. The uncertainty in the electronic cross section generated in the remaining partially resolved bands due to band overlap is less than 10%, since most of the strong overlap occurs for bands of the same band system from different v' progressions. Thus the total uncertainty for electronic cross sections of the b' and c_4' states is 25%. For certain progressions the uncertainty is larger. The results for electronic emission cross sections would have been severely degraded at any lower resolution.

The effect of the N I lines on the 100-eV spectrum is a very important consideration, since many of the candidate features arise from N I and N II transitions. A comparison of Fig. 9 and 10 provides the most direct answer. We see that at 20 eV, an energy below the dissociative excitation threshold of the N I lines, that the spectrum remains virtually unchanged in relative intensity. Thus N I and N II emissions are not important in the euv spectrum of N_2 for wavelengths 92–102 nm. The only exceptions are features 24*A* and 24*B*, which are predominantly N I resonance lines. Feature 24*A* is entirely due to N I emission and 24*B* contains a small amount of b' emission most notably from the (8,2) band at 95.3 nm. The N I($g\ ^4S^\circ - ^4D$) multiplet with a mean wavelength of 95.24 nm was used to establish the wavelength scale. The only other N I contribution of greater than 10% to the intensity in this wavelength region comes from N I ($g\ ^4S^\circ - ^4P$) for features 24*F* and 24*G* discussed in the preceding section. A small double peak in 24*G*, the stronger of the N I features between 24*F* and 24*G*, shows a closely spaced double peak. The cross sections of the N I features are about 5×10^{-19} cm^2 and 1×10^{-19} cm^2 for combined features 24*A*, 24*B* and 24*F*, 24*G*, respectively. The total cross section of 127×10^{-19} cm^2 at 100 eV for features 22–26 inclusive, given in Table I, is mostly contributed by c_4' bands. The only features from molecular transitions from bands other than the c_4' bands in the 92–120 nm spectral region are indicated in Table III. These are features from b' bands with a total cross section of $\sim 7.4\times10^{-19}$ cm^2 and the $b(1,1)$ band, feature 26*D*, has a cross section of 1.2×10^{-19} cm^2. Roughly 90% of the emission cross section in this wavelength region arises from transitions in the c_4' band system. Therefore the b' and b states must be heavily predissociated to account for weak contributions or even absence in emission of corresponding bands in this spectral region. This point becomes obvious when we compare the magnitudes of the excitation cross sections to the emission cross sections.

THE $c_4'\ ^1\Sigma_u^+ \rightarrow X\ ^1\Sigma_g^+$ CARROLL-YOSHINO BAND SYSTEM

Figure 11 shows a comparison of the experimental and synthetic spectra for the c_4'-$X(v'=0-4, v'')$ progressions. Each progression is normalized to the strongest transition for unperturbed Franck-Condon factors. In addition, the $v'=6$ progression, not shown, is identified as a strong contributor to the experimental spectrum. The $v'=5$ progression is not seen in this work nor by Roncin, Launay, and Yoshino. However, Yoshino[53] has observed the $c_5'(5,0)$ band and reports the $v'=5$ absorption cross section to be very weak. The analysis of Stahel, Leoni, and Dressler[10] reports the $v'=5$ excitation cross section to be only $\sim 2\%$ of the $v'=4$ value. The overplot in Fig. 11 is useful to show that the high v' levels with $v'=3,4,6$ have much higher excitation rates than the unperturbed Franck-Condon factors used to generate Fig. 8 would predict. For example, in the neighborhood of 96 nm the (0,0), (1,1), and (2,2) bands fall off normally with intensity in the experiment, in crude agreement with the Franck-Condon factors, but the (3,3) and (4,4) bands along with the (6,5) and (6,7) are orders of magnitude stronger than without the perturbation from the b' state. In fact, Stahel, Leoni, and Dressler have shown the $v'=3,4,6$ levels have unperturbed transition moments that are too small to interfere with the levels they are in near resonance with. Their large excitation rates can be traced to constructive interference from nearest neighbors above and below the resonance. For example, $v'=4$ has a large eigenvector contribution from b' (13,14). Thus Eq. (8) must be generalized to include a three-level interaction.

Table II is the most important overall result for the c_4' state. We estimate the cross section for each observed band of the Carroll-Yoshino series. A comparison between the emission-cross-section results presented here and the electron-scattering excitation-cross-section results of Geiger and Schroder[2] is shown in Table II. This data set is derived from the individual experimental cross sections. It serves to show that predissociation is small ($< 10\%$) for the c_4' state. We consider each of the c_4' progressions in order from $v'=0$ to 6. Feature numbers 27–38 are described in Ref. 3. In Table II we include the cross-section results that apply to the c_4' bands. These features contribute less than 1% of the electronic cross section.

Table II shows that the $v'=0$ progression contributes about 73% of the c_4' cross section at 100 eV. This value is in close agreement with the results of Geiger and Schroder who find that the $v'=0$ progression contributes about 78% of the excitation cross section. The total cross section at 100 eV for the $v'=0$ progression is 88.8×10^{-19} cm^2. This value is based on the summation of cross sections for features 24*C*, 25*A*, 26*A*, etc. The (0,0) band is the strongest band with a value of 74.7×10^{-19} cm^2. The intensities in the band fall off much slower than the branching ratios from calculations based on the Franck-Condon approximation. This comparison is made in the columns labeled relative *Q*, experiment, and theory. The identification of these bands is unambiguous. Contributions from blending transitions in the measurement bandwidth are less than 10%. For example, the cross-section contribution from the $b'(7,2)$ band to the total cross section of the $c_4'(0,0)$ band, feature 24*C*, is estimated to be $\sim 1\times10^{-19}$ cm^2, about twice the

TABLE III. Analysis $X\,^1\Sigma_g^+ \rightarrow b'\,^1\Sigma_u^+$ excitation.

(a) Resonance bands

$b'\,^1\Sigma_u^+$ v'	Feature No.	Franck-Condon factor RKR	Emission cross section this work 20 eV $Q(10^{-19}$ cm$^2)$	Emission cross section this work 100 eV Q $(10^{-19}$ cm$^2)$	Approximate emission cross section of progression[b] -100 eV Relative arb. units	Approximate emission cross section of progression[b] -100 eV Absolute Q $(10^{-19}$ cm$^2)$	Excitation cross-section-energy loss scattering Relative (arb. units) Ref. 2	Ref. 18	Ref. 10	Absolute $(10^{-19}$ cm$^2)$ 100 eV[h]
3		0.000 12								1.0
4		0.000 44							0.009	
5		0.0013					0.004	0.003	0.004	0.06
							0.0082			
6		0.0031						0.0056	0.005	1.16
7		0.0069					0.0		0.008	1.47
8		0.0132					0.0		0.011	0.90
9	$20D$[a,c]	0.0225					0.011		0.027	4.03
10	$20A$[c]	0.0353	<0.08	<0.38	<0.15	<1.23	0.004	0.023	0.015	0.69
11	$19E$	0.0502	0.32	0.49	0.12	0.99	0.0086	0.0078	0.045	1.48
12	$19D$[c]	0.0660	<0.65	<1.27	<0.23	<5.06	0.071	0.068	0.072	12.41
13	$19C$[a,c]	0.0807	1.04,0.07	2.98,0.21	0.025	0.71	0.011	0.0019	0.043	1.80
14	$19A$[a]	0.0918	0.12	0.57	0.069	1.54	0.0918	0.092	0.092	16.79
15	$18C$[a]	0.0973	0.14	1.07,0.46	0.12	1.10	0.105	0.106	0.109	21.82
16	$18A$	0.0967	0.75	2.14	0.21	4.74	0.141	0.146	0.156	26.71
17	$17G$	0.0912	0.08	0.19	0.018	0.40	0.076	0.080	0.077	14.50
18	$17D$	0.0807	0.04	0.16	0.015	0.37	0.072	0.007	0.013	1.30
19	$17C$[c]	0.0681	~0.04	~0.15	~0.015	~0.037	0.041	0.045	0.052	8.23
20		0.0548	<0.05	<0.05			0.035	0.039	0.039	6.97
21		0.0420	<0.05	<0.05			0.0	0.0	0.012	
22		0.0310	<0.05	<0.05			0.011	0.011	0.017	2.06
23		0.0219	<0.05	<0.05			0.017	0.019	0.023	3.48
24		0.0151	<0.05	<0.05			0.0067	0.008	0.012	1.40
25		0.0102	<0.05	<0.05					0.001	
Total:[f]			2.0	5.2		13.0				128.2

(b) Nonresonance bands

Feature No.	$b'\,^1\Sigma_u^+(v',v'')$	Blending of bands	20-eV cross section $(10^{-19}$ cm$^2)$	100-eV cross section $(10^{-19}$ cm$^2)$
$20B$	$b'(13,1)+b'(17,2)$		0.03	0.10
$20D$	$b'(9,0)+b'(16,2)$		0.63	1.15
$20E$[a]	$b'(12,1)$	$c_4'(6,3)$ weak	0.48	1.69,1.59
$21A$[a]	$b'(11,1)$		0.35	6.65,0.54
$21B$	$b'(14,2)$		0.11	0.49
$21C$	$b'(13,2)$		0.02	0.06
$22A$	$b'(9,1)+b'(16,3)$		0.84	1.42
$22C$	$b'(8,1)$		0.087	0.19
$23A$	$b'(7,1)$		0.26	0.47
$23F$	$b'(16,4)+b'(9,2)$		0.69	1.09
$24B$[a]	$b'(8,2)+b'(11,3)$	(11,3) very weak	0.15	3.84,0.50
$24C$	$b'(7,2)$		0.03	1.0
$24H$	$b'(6,2)+b'(9,3)$	$c_4'(6,6)$	<0.23	<0.86
$24I$	$b'(12,4)+b'(19,6)$	(19,6) weak	0.22	0.35
$25E$	$b'(16,6)$		0.18	0.25
$25G$	$b'(9,4)$		0.37	0.96
$25H$	$b'(12,5)$		0.13	0.21
$26E$	$b'(16,7)$		0.83	1.03
$26G$	$b'(9,5)$		0.38	0.51

TABLE III. (*Continued*).

(b) Nonresonance bands

Feature No.	$b'\,^1\Sigma_u^+(v',v'')$	Blending of bands	20-eV cross section (10^{-19} cm^2)	100-eV cross section (10^{-19} cm^2)
27*F*	$b'(9,6)+b'(6,5)$	(9,6) strongest	0.33	0.57
27*G*	$b'(12,7)$		0.15	0.20
27*I*	$b'(8,6)+b'(5,5)$		0.06	0.12
27*J*[a]	$b'(11,7)$		0.10	0.78,0.15
28*D*	$b'(3,5)+b'(9,7)$	$(3,5)+b(1,3)$	0.46	1.11
29*A*[a]	$b'(11,8)$		0.11	0.96,0.17
Total			7.1	14.7
			9.1	19.9

Total[f] measured b' cross-section resonance plus nonresonance bands—this work

(c) Emission cross section at 100 eV for v' progressions between 7 and 19.

v' \ v''	0	1	2	3	4	5	6	7	Progression emission cross-section total	Emission yield (%)
				Q (10^{-19} cm^2)						
7		0.47	1.0						1.47	
8		0.19	0.40[i]				0.06[i]		0.65	
9	0.58[i]	0.71[i]	0.55[i]	0.21[i]	0.96	0.51	0.28[i]	0.10[i]	3.9	97
10	0.19								0.19	19
11	0.49	0.54		0.10[i]				0.15	1.45[j]	~100
12	0.63[i]	1.59			0.35[i]	0.21		0.20	2.98	16
13	0.21	0.05[i]	0.06						0.32	12
14	0.57		0.49						1.06	6
15	0.46								0.46	2
16	2.14		0.58[i]	0.71[i]	0.55[i]		0.25	1.03	5.26	20
17	0.19		0.05[i]						0.24	2
18	0.16								0.16	12
19	0.15								0.15	2

[a]Evidence for N I line overlap at 100 eV.

[b]All relative values normalized to $v'=14$ value of RKR Franck-Condon Factor, Ref. 10.

[c]Band overlap c_4', c_5', o_3, or b' ($v''\neq 0$). See Stahel, Leoni, and Dressler, Ref. 10 for % overlap of excitation cross section of resonance bands, e.g., $b'(13)=43.9\%$, $b'(16)=98.9\%$.

[d]Geiger and Schroder, Ref. 2.

[e]Stahel, Leoni, and Dressler, Ref. 10.

[f]Total b' cross section at 100 eV, corrected for N I and N II lines or c_4' band overlap, second entry in 100-eV emission column is estimated b' cross section. Entry with less-than sign contributes 50% total cross section.

[g]Zipf and McLaughlin, Ref. 18.

[h]Modified Born Approximation (this work) based on optional oscillator strength of this work.

[i]Blended b', c_4', o vibrational cross sections assigned 50%±40% to each transition.

[j]Includes $b'(11,8)$ contribution of 0.17.

(7,1) band cross section. The cross-section contribution of the $b'(14,4)$ band to the total cross section of the $c_4'(0,0)$ band cross section is estimated to be $\sim 1\times 10^{-20}$ cm^2, about $\frac{1}{5}$ of the $b'(14,0)$ band cross section from Franck-Condon approximation branching-ratio considerations. The b' cross sections are given in Table III and will be discussed in the next section. The relative cross sections of the transitions of the $v'=0$ progression are preserved at 20 eV with a total cross section of 24.6×10^{-19} cm^2.

The $v'=1$ and 2 progressions are very weak. The strongest features for these progressions are the (1,1) and (2,2) bands. The total cross sections for each of these progressions are down almost two orders of magnitude from the $v'=0$ progression. Each of the features in the progression, except for the (2,1) and (2,2) bands, may contain some contribution from the overlapping b' bands, although in all cases Roncin, Launay, and Yoshino indicate

that the contributions of these overlap features are very weak. The contribution of the $b'(17,5)$ band to the $c_4'(1,1)$ band could be as large as 0.3×10^{-20} cm^2, based on a branching-ratio comparison to the (17,0) band, feature 17*G*. However, Roncin, Launay, and Yoshino[17] report the $c_4'(1,1)$ band as much stronger than the $b'(17,5)$ band or the $c_3(2,2)$ band. The spectrum in Fig. 9 shows that the $c_4'(2,1)$ band peak is resolved. On that basis an approximate cross section is given. Roncin, Launay, and Yoshino report the $c_4'(1,1)$, (2,1), and (2,2) bands as strong emissions.

The c_4'-X $v'=3$ progression begins a trend showing a strong reversal in cross section from the predicted Franck-Condon factors for direct excitation. The two strongest peaks are the (3,2) and (3,3) bands, both of which are essentially unblended. The contribution of the $b'(13,3)$ band to feature 23*D* containing the $c_4'(3,2)$ band is less than 0.05×10^{-19} cm^2. The total cross section of feature 23*D* is 2.04×10^{-19} cm^2. The $c_4'(3,5)$ band is feature 26*C* and is blended with the $c_4'(4,6)$. Both features are reported as very strong in Ref. 17. We arbitrarily attribute half the cross section in 23*C* to each of the two features. The total cross section of the $v'=3$ progression is $\sim6.9\times10^{-19}$ cm^2. This value for the $v'=3$ cross section is 5.7% of the total c_4' cross section and once again is in good agreement with the electron-scattering results of Geiger and Schroder, who find a value of 5% for the contribution to the excitation cross section. By contrast, the Franck-Condon factors predict that the $v'=3$ progression contributes about 2×10^{-6} of the total cross section.

The cross section for the $v'=4$ progression has an es-

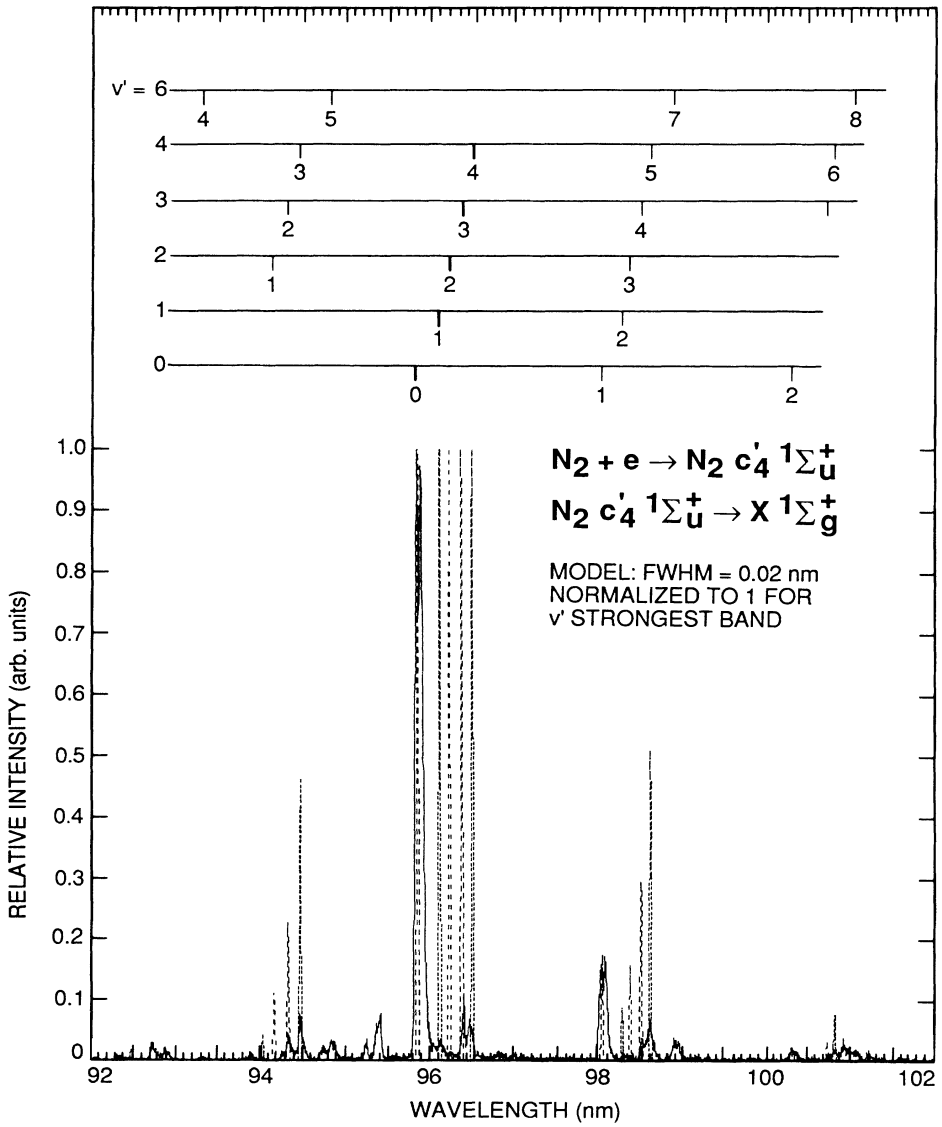

FIG. 11. Calibrated optically thin spectrum of N_2 from Fig. 9 overplotted with model of $c_4'\,{}^1\Sigma_u^+ \rightarrow X\,{}^1\Sigma_g^+$ band system from Fig. 8 for $v'=0,1,2,3,4$ progressions normalized to peak value in each progression. The model data were normalized to unity for each progression separately to bring strongest features on scale.

timated value of 14.0×10^{-19} cm^2 at 100 eV. The strongest band is the (4,3), but the (4,4) and (4,5) are also quite strong. The $c'_4(4,0)$ and $c'_4(4,1)$ band cross sections are estimated from the 0.05-nm resolution spectra for the wavelength region below 92 nm used in the analysis of the b'-X band system. The cross section of the $c'_4(4,4)$ band is determined from the cross section for this feature from the 20-eV spectrum. The cross section of the $c'_4(4,5)$ band, feature 25*D*, is estimated from the measurement of the $b(1,1)$ band cross section, feature 26*D*. We find that the cross section of the $b(1,1)$ band is 1.18×10^{-19} cm^2 at 100 eV and 0.62×10^{-19} cm^2 at 20 eV. On the basis of branching ratios, the $b(1,0)$ and $b(1,1)$ are expected to be about of equal intensity. The blending between the $c'_4(4,0)$ and $b'(13,0)$ bands in feature 19*C* is handled by noting in the electron-impact-excitation experiment that the $b'(13,0)$ band is only 7% of the combined cross section. Thus the 20-eV cross section of feature 19*C* must contain a small contribution from the $b'(13,0)$ band. The $v'=4$ progression contributes 12% of the measured cross section of the c'_4 state, in excellent agreement with the value of 13% from Geiger and Schroder.[2]

The $v'=5$ level is neither observed nor resolved from the $b'(16,0)$ band but is expected to be relatively weak. The mean value for the cross section of the $v'=6$ level is 8.2×10^{-19} cm^2. The most intense features for this progression are the (6,5) and (6,7) bands, features 23*G* and 25*F*, respectively. The (6,0) and (6,1) bands are resolved in the 0.05-nm FWHM spectra of a subsequent section describing the analysis of the b' band system, and the contribution of the blended $b'(19,0)$ band to feature 17*C* is small due to perturbations for b' ($v'>17$). This destructive interference effect is explained in Stahel, Leoni, and Dressler.[10] Stahel, Leoni, and Dressler have pointed out that the local resonance between the c'_5 state for $v'=0$ and the b' state for $v'=15-19$ strengthens the bands below and weakens the bands above the resonance between $v'=17$ and 18. The intensity envelope in the vicinity of these bands in the excitation experiment resembles a Fano profile.

MEDIUM-RESOLUTION SPECTRUM 83–92 nm: THE BIRGE-HOPFIELD-II BAND SYSTEM $b'\,^1\Sigma_u^+ \rightarrow X\,^1\Sigma_g^+$

For energies above 100 eV the excitation cross section of the b' state is comparable to the c'_4 state excitation cross section. The electron-scattering spectrum of Geiger and Schroder[2] shows comparable intensities for the two states. The only previous emission cross-section study of the b' state[18] reports a predissociation fraction of 0.83 for the entire electronic transition $0<v'<21$. With the

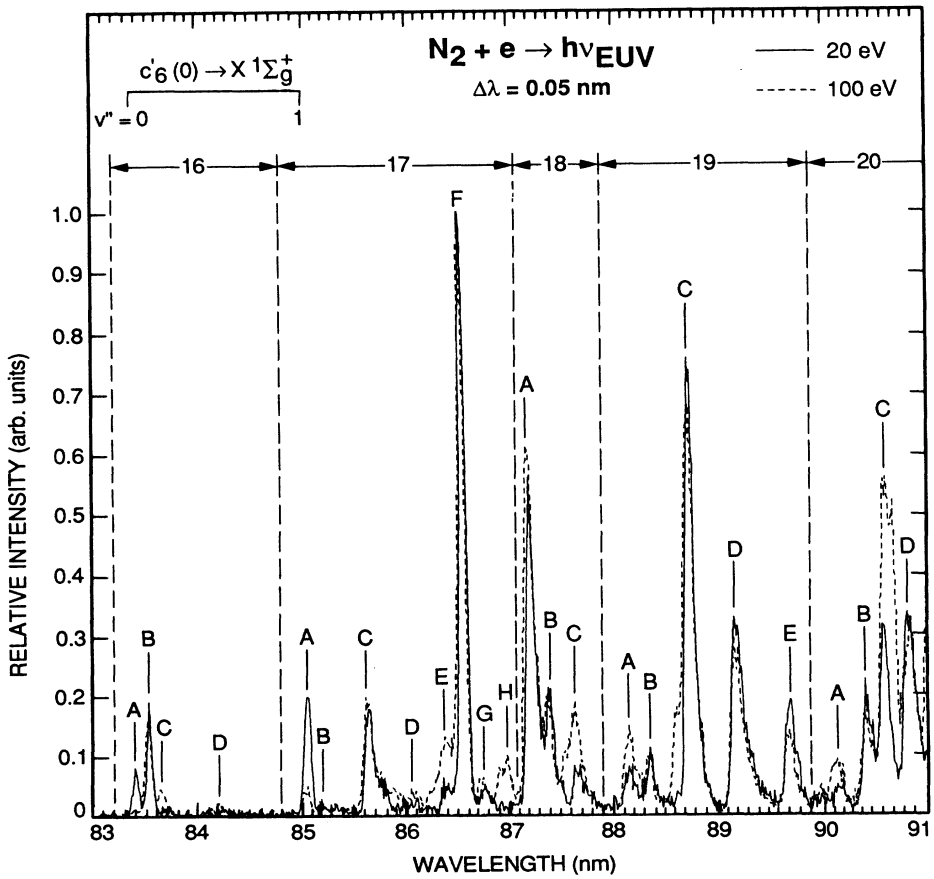

FIG. 12. Calibrated optically thin spectrum of N_2 from 83 to 91 nm produced by electron impact at 20 eV (——) and 100 eV (— — —) at 0.05-nm resolution. The feature numbers and letters are identified in Table I.

availability of high-resolution identifications of the b' state[17] we reinvestigate the emission cross section of this state between threshold and 400 eV, and with the modified Born approximation,[22] extend the results to arbitrary high energy. In addition, we analyze the 0.05-nm resolution spectra at 20 and 100 eV and "count all the photons" from the b' state to get a total electronic cross section.

An overplot of the electron-impact-induced fluoresence spectrum at 20 and 100 eV measured at a resolution of 0.05 nm is shown in Fig. 12. This figure is useful in the analysis of the $b'\,^1\Sigma_u^+ \rightarrow X\,^1\Sigma_g^+$ BH-II band system, since all the intense bands appear in this wavelength region. The wavelength range of Fig. 12 is from 83 to 91 nm. The signal-to-noise ratio is high enough to easily ascertain the location of N I and N II features. For example, N I lines between 83 and 92 nm are noted at 86.5, 86.9, 87.7, 88.3, 90.6, and 91.6 nm (making use of Fig. 13). All other features, roughly 90% of the integrated cross section of the spectrum at 100 eV, are molecular bands.

A useful comparison of the deperturbed b' model included without rotational structure and the 100-eV spectrum is given in Fig. 13. The 100-eV data are shown over the wavelength range 85–92 nm. The $v''=0$ progression band origins are indicated. It is clear from this figure that the relative intensities based on direct excitation without perturbations do not match the observed spectrum. Many of the features are very weak but discernable, indicating that predissociation may be important. From our observations the b' bands break off in emission at $v'=20$ at the $^2D^0+^2D^0$ dissociation limit. This is the vibrational level separating weak and strong predissociation.

In agreement with the Rydberg-Klein-Rees (RKR) Franck-Condon factors in Table III(a) and the electron scattering spectra,[10,18] $b'(16,0)$ is the strongest transition. Although a higher-resolution observation will be shown to be important for complete separation of all the b' and c_4' transitions, it is still possible to obtain the b' electronic emission cross section. However, it is more difficult to

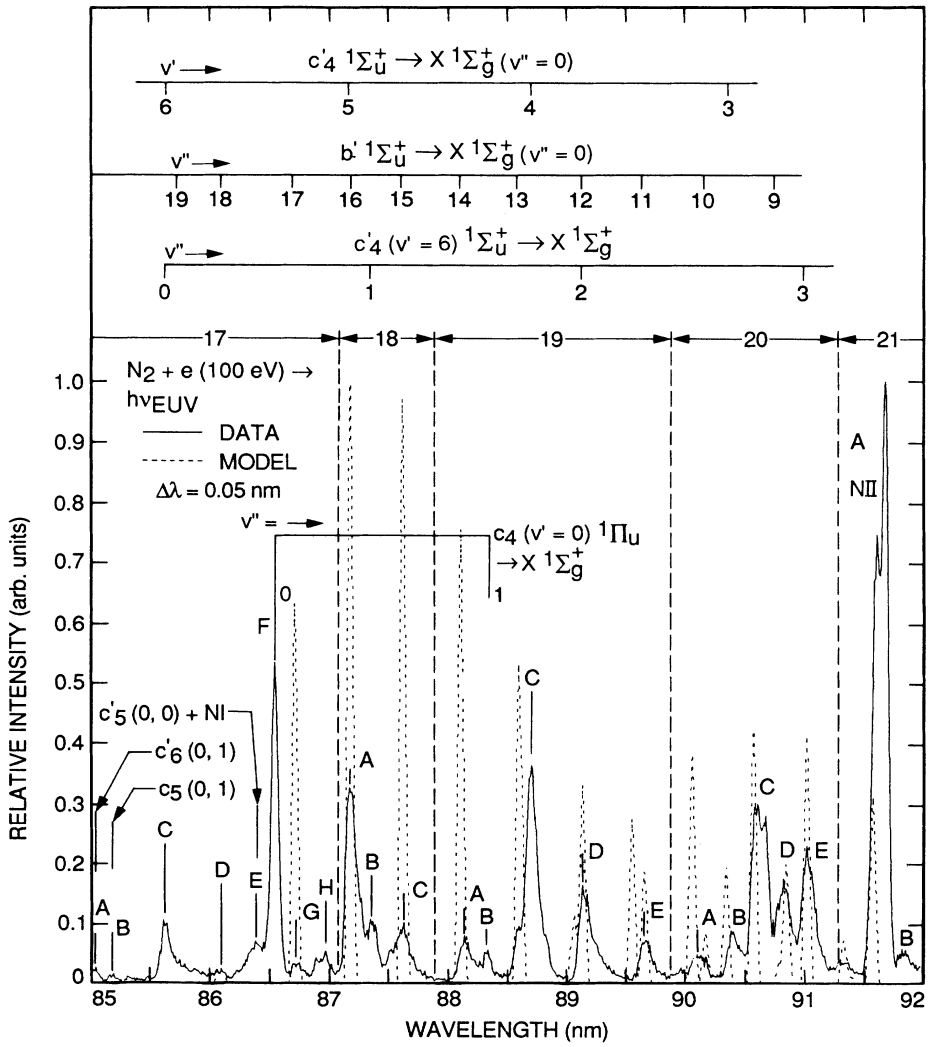

FIG. 13. Calibrated optically thin spectrum of N_2 from 85 to 92 nm produced by electron impact at 100 eV overplotted with synthetic spectrum of Fig. 8 for the $b'\,^1\Sigma_u^+ \rightarrow X\,^1\Sigma_g^+$ BH-II band system. Data and model are at 0.05-nm resolution.

obtain the cross sections of each v' progression, since b' bands from different progressions are overlapped. The low value for the $b'(v',0)$ emission cross sections and the necessity to avoid self-absorption brought about by the use of higher gas pressures prompted the measurement at 0.05-nm resolution in this wavelength range. Spectra were obtained at 6×10^{-6} and 2×10^{-5} Torr and found to have identical relative intensities. The 2×10^{-5}-Torr spectra at 20 and 100 eV are presented in Figs. 12 and 13.

The analysis of the 20- and 100-eV cross sections from the spectra in Figs. 9, 10, 12, and 13 is given in Tables III(a)–III(c). In Table III(a) we list the relative excitation cross sections of the two electron scattering experiments normalized to the $v'=14$ unperturbed Franck-Condon factor. These two electron scattering experiments are in excellent relative agreement. The experimental results reported by Zipf and McLaughlin[18] were performed at 200 eV; the experiment by Geiger and Schroder[2] was accomplished at 25 keV. The excitation cross section at 100 eV based on our results using the modified Born approximation is given. Zipf and McLaughlin do not give any individual band or progression emission cross sections. It is not possible to compare the detailed analysis of each emission experiment.

A direct comparison between the emission work presented here and the electron scattering work in Table III(a) is not possible without branching ratios for the $v''=0$ progression. The $v''=0$ progression is the strongest progression and is well separated from the strong c'_4 vibrational bands. A first-order calculation of the cross section of the v' progressions on the basis of unperturbed Franck-Condon factors for branching ratios is given. This calculation indicates that the $v''=0$ transitions are roughly 25–50 % of the intensity in v' progressions for $9<v'<19$.

Table III(a) shows that the (12,0) band is blended with the $c'_4(6,2)$ band, albeit the c'_4 band is declared weak by Ref. 17. In a similar way, the $b'(10,0)$ band is overlapped by the $o_3(4,1)$ band. Figure 12 shows the effect of the $o_3(4,1)$ band on the spectrum. The relative cross section of feature $20A$ is different from $19E$, the $b'(11,0)$ band. Since $b'(18,0)$ is very weak, the contribution of $b'(18,2)$ to the $b'(11,0)$ band is negligible. The branching ratio of the (18,2) band is much smaller than the (18,0) band on the basis of the Franck-Condon approximation. Roncin, Launay, and Yoshino observe $b'(18,2)$ as very weak. The contribution of the $b'(18,2)$ band to feature $19E$ is negligible. Both the $b'(12,0)$ and $b'(10,0)$ cross sections are given as upper limits. For the purpose of calculating a total cross section, we arbitrarily attribute half the cross section of these features to each band. Resonance bands overlapped by N I lines are $b'(13,0)$ and $b'(15,0)$. These vibrational bands have their 100-eV cross sections determined from the 20-eV spectrum and the $b'(16,0)$ excitation function discussed below. The other resonance bands are resolved except for $b'(9,0)$.

With these assumptions, Table III(a) demonstrates two important results. First, the emission cross section of the b' electronic cross section is about 13×10^{-19} cm^2 for $v'>9$. Second, the predissociation fraction increases with increasing vibrational quantum number. To more accurately check these values we make use of Tables III(b) and III(c), which contain the remainder of the vibrational features identified as arising from the b' state.

Table III(b) lists the cross section of the b'-X $v''>0$ bands observed in this experiment, along with the blended (9,0) band. The total cross section is 19.9×10^{-19} cm^2 for all b'-X features. The contribution of a few b' features above 102 nm from Ref. 3 is included in the analysis. The principal uncertainty in Table III(b) is the blending of the $c'_4(6,6)$ band with the $b'(6,2)$ and $b'(9,3)$ bands.

Table III(c) is an estimate of progression cross sections in order to deduce approximate emission and predissociation yields for each level. Table III(b) shows that many b' bands are blended with one another. We arbitrarily attribute in most cases half the intensity to each b' feature. The results are consistent with Table III(a). First, the emission yield decreases with vibrational quantum number. Emission yields for $v'=9$ and 11 are about 100%. For $v'>12$ the emission yield is between 2 and 20%. The progression with the largest emission-cross-section is $v'=16$. Six features are attributed to the $v'=16$ progression with 26% of the total electronic emission cross section. The $v'=9$ progression has eight observable features with 20% of the cross section. Predissociation appears to increase with increasing vibrational quantum number. Helm and Cosby[32] have analyzed the predissociation of $v'=16$ and $17F$. It is found that ~95% of these predissociations arise from the $N(^4S^\circ)+N(^2D^\circ)$ limit. The remainder populate the $N(^4S^\circ)+N(^2P^\circ)$ limit. We estimate the overall predissociation yield for the b' state to be 84%.

THE $np\sigma\ ^1\Sigma_u^+$, $n=5,6$ AND $np\sigma\ ^1\Pi_u$, $n=4,5$ EMISSION CROSS SECTIONS

In addition to the b' and c'_4 band systems which arise from excitation of the emission electron to the valence state and lowest member of the $np\sigma$ Rydberg series with $n=3$, higher members of the $np\sigma$ Rydberg series are observed in this experiment with $n=4$ and 5. The analogous b and c_n series are the valence state and lowest member of the $np\pi$ Rydberg series. We observe the $n=4$ and 5 members. Both Rydberg series ultimately converge to the $X\ ^2\Sigma_g^+$ ground state of the ion. None of these higher-member Rydberg series has been reported in previous electron-impact-emission measurements. The relationship between the running index number for the Rydberg series and the principal quantum number of the Rydberg electron is the same number for the $np\pi$ series, and the running index number is always one more for the $np\sigma$ Rydberg series. This problem has led many authors to drop the n subscript and choose instead the notation of Ref. 10. Keeping this in mind, we prefer keeping the n subscript for historical reasons.

Geiger and Schroder[2] report excitation peaks for the higher-member Rydberg series, c'_5, c_4, and c_5 electronic states, but no analysis is given. Table IV gives the cross sections of the four other electronic states observed in our experiment. The largest emission cross section for an N_2 molecular band for wavelengths below 91 nm at both

TABLE IV. Other important emission cross sections at 20 and 100 eV.

State	v'	v''	Feature No.	Absolute emission cross section (10^{-19} cm^2) 20 eV	100 eV
$c_6' {}^1\Sigma_u^+$	0	0	16A	0.063	0.022
$c_6' {}^1\Sigma_u^+$	0	1	17A	0.21	0.10
$c_5 {}^1\Pi_u$	0	0	16B	0.15	0.37
$c_5' {}^1\Sigma_u^+$	0	0	17E	0.064	0.54[a]
$c_4 {}^1\Pi_u$	0	0	17F	0.99	2.33
$c_4 {}^1\Pi_u$	0	1	19B	0.15	0.29

[a]Possible N I line overlap at 100 eV.

20 and 100 eV is the $c_4(0,0)$ transition, feature 17F, at 86.53 nm. The $c_4(0,1)$ band is also observed. The total emission cross section of these two features is 2.62×10^{-19} cm^2. No other c_4 bands are observed.

Cross sections for the (0,0) bands for the c_5' and c_6' band systems are also given. In addition, the $c_5'(0,1)$ band is also observed. Its cross section given in feature 17A is larger than the (0,0) band in feature 16A. The total observed cross section for the c_6' state at 100 eV is 0.12×10^{-19} cm^2. On the other hand, the $c_5'(0,1)$ band overlaps the $b'(14,0)$ band, but is measured to be very weak by Roncin, Launay, and Yoshino. The emission cross section of the $c_5'(0,0)$ band is 0.064×10^{-19} cm^2 at 20 eV. Due to the N I line overlap at 100 eV, the cross section of the $c_5'(0,0)$ band is only roughly estimated to be 0.2×10^{-19} cm^2 at 100 eV.

The c_4 and c_5' states have been observed to be highly predissociated by Helm and Cosby.[32] The branching of the fragments to the $N(^4S^\circ)+N(^2D^\circ)$ and $N(^4S^\circ)+N(^2P^\circ)$ excited atom limits is strongly dependent on the rotational level and parity from vibrational level $v'=0$.

THE 95.8-nm TRANSITION, $c_4' {}^1\Sigma_u^+ (v'=0)-X {}^1\Sigma_g^+ (v''=0)$

In the euv the (0,0) transition of the $c_4' {}^1\Sigma_u^+-X {}^1\Sigma_g^+$ band system is the most intense feature produced in electron-impact excitation of N_2 in an optically thin source, and its emission cross section (74.7×10^{-19} cm^2) rivals that of N_2^+ (391.4 nm; 180×10^{-19} cm^2) at 100 eV.[48] The total emission cross section of N_2 in the wavelength region from 82 to 102 nm studied at high resolution in this paper is 155×10^{-19} cm^2. The $c_4'(0,0)$ vibrational feature represents 48% of the energy radiated in this wavelength range. Thus further work is warranted to develop a complete model for the band system.

A modified Born approximation[22] of the laboratory cross-section data gives a second method of providing an absolute excitation function. The modified Born approximation formulation utilizes the fact that the optical oscillator strength is proportional to the excitation cross section at high energy. This technique provides a means of comparing excitation and emission cross sections. If oscillator strengths are not available, it is possible to use the modified Born approximation with our relative flow results to obtain a value.

We show the excitation function of the 95.8-nm transition in Fig. 14. The figure shows a comparison with the results of Morgan and Mentall[19] and Zipf and McLaughlin.[18] We list the digital values of the relative cross section in Table IV. The cross section peaks at about 70 eV. The agreement between the various experiments for the relative energy dependence is 10%. For many purposes it is desirable to have an analytical model of the absolute cross section. The absolute oscillator strength for the (0,0) transition has been measured by Lawrence, Mickey, and Dressler[23] to be $f_{00}=0.14\pm0.04$. The lifetime of the $v'=0$ level has been measured by Hesser and Dressler[24] to be $\tau=0.9\pm0.2\times10^{-9}$ s ($f_{00}=0.128$, based on our branching ratio of 0.84). With this information we have an independent means of measuring the absolute cross section. We list in Table V three estimates of the Q_0 excitation cross section. The difference between our relative flow result and the modified Born approximation result using the Lawrence, Mickey, and Dressler[23] oscillator strength is 10.8% and 20% from the f_{00} value of Hesser and Dressler.[24] Both results fall within the uncer-

TABLE V. Emission cross sections of N_2 ($c_4' {}^1\Sigma_u^+ \rightarrow X {}^1\Sigma_g^+$).

(a) Relative emission cross section 95.8-nm (0,0) band.

Energy (eV)	Relative cross section (arb. units)
12.93	0
14	0.04
15	0.06
16	0.10
18	0.18
20	0.27
22	0.35
25	0.47
30	0.64
35	0.72
40	0.80
50	0.92
60	1.00
70	1.00
80	0.99
90	0.98
100	0.94
120	0.89
150	0.80
250	0.72
300	0.65
350	0.62
400	0.56

(b) Absolute emission cross section $v'=0$ at 100 eV.

Method	Q (10^{-19} cm^2)
This work—relative flow	88.8
This work—modified Born approximation and Ref. 23.	79.4
This work—modified Born approximation and Ref. 24.	72.6

tainty of this experiment. The comparison suggests predissociation of the $v'=0$ level is less than 10%. This result is in agreement with the analysis of the $v'=0$ level presented in Table II, showing a 5% difference between the electron-scattering results of Geiger and Schroder[2] and the emission results of this work.

Based on the excellent agreement between the results here and those of Lawrence, Mickey, and Dressler,[23] we recommend that the oscillator strength of the c_4' be determined by our cross-section measurements since our results have the least uncertainty of 22%. The oscillator strength for the $c_4'(0,0)$ transition is $f_{00}=0.156\pm0.03$. The band-system electronic oscillator strength f_0 is found to be 0.223 and is calculated from the expression

$$f_0=\sum_{v'} f_{ov'} . \tag{10}$$

We show the modified Born approximation fit to the data (converted to collision strength Ω) using the absolute oscillator strength from this experiment in Fig. 14. The constants used in this formulation are given in Table VII.

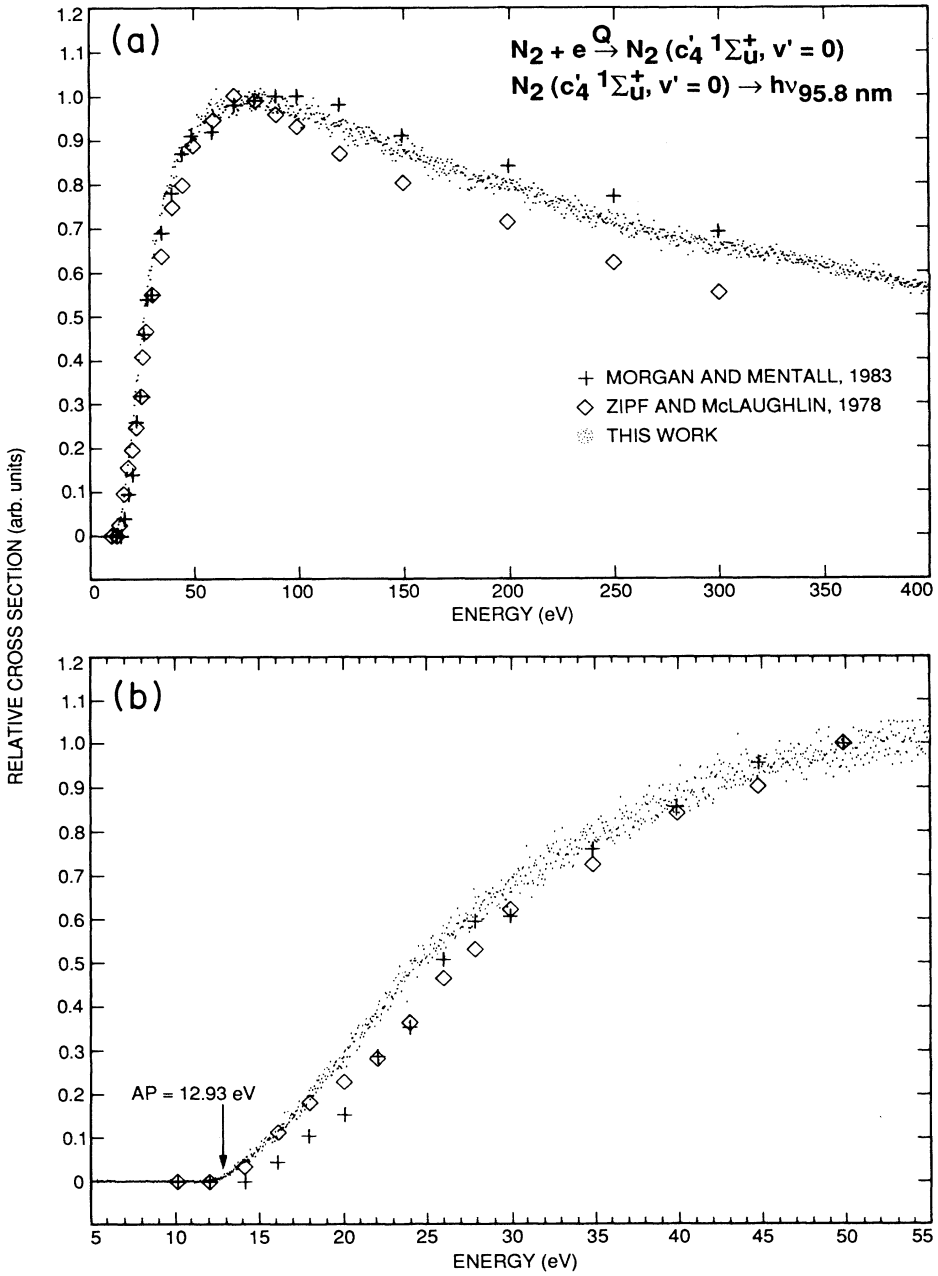

FIG. 14. (a) Relative emission cross section of the $c_4' {}^1\Sigma_u^+(0,0)$ band from 0–400 eV compared to Morgan and Mentall (Ref. 19) (+) and Zipf and McLaughlin (Ref. 18) (◇). Data points are taken every ~0.4 eV. (b) Relative emission cross section of the $c_4' {}^1\Sigma_u^+(0,0)$ band from 0–55 eV. Data points are taken every ~50 meV.

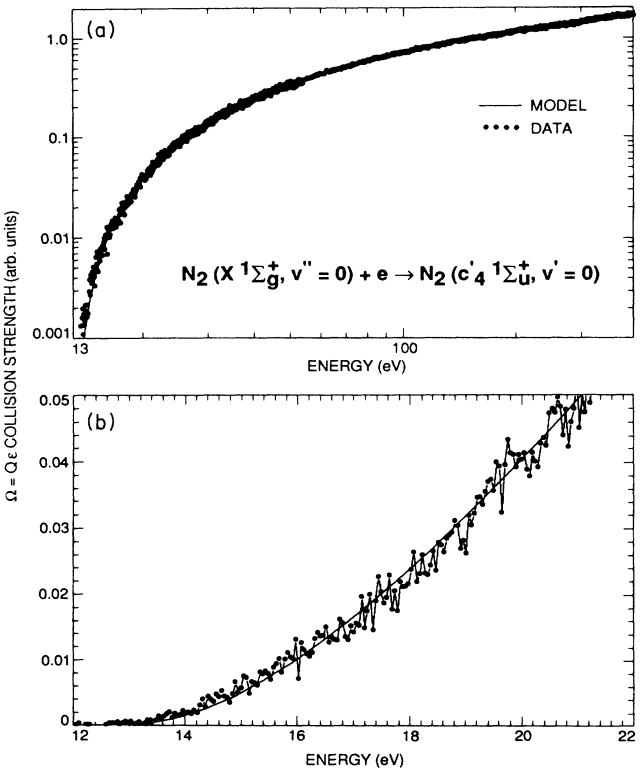

FIG. 15. Collision strength of the $c'_4\ ^1\Sigma_u^+(0)$ vibrational level model (solid line) and data (dots) plotted against energy and normalized to an oscillator strength of 0.1567 from Table VII(a) for $v'=0$ (a) 13–400 eV and (b) 12–22 eV.

Table VII is discussed in the final section of the paper.

The advantage of the modified-Born-approximation model is that the formula is accurate at all energies including the threshold region. Note the degree to which the model and data fit in Fig. 15 in the vicinity of the threshold region as well as the high-energy region.

THE $b'\ ^1\Sigma_u^+$ ($v'=16$)→$X\ ^1\Sigma_g^+$ ($v'=0$) BAND-EMISSION CROSS SECTION

The strongest b' emission band is the $b'(16,0)$ transition at 87.14 nm. It lies very close to the $c'_4(6,1)$ transition at 87.35 nm. We have measured the $b'(16,0)$ excitation function shown in Fig. 16 over the energy range 0–400 eV. The spectrometer resolution was set in two separate experiments at 0.05 and 0.08 nm to isolate the (16,0) band. Excitation-function measurements at the two resolutions were identical. The measurement at 0.08 nm is shown in Fig. 16. The values of the relative cross section are shown in Table VI. The cross section peaks at 65-eV energy. The ratio of 20 to 100-eV cross sections is given in Table VI to be 0.27. This ratio is used in the analysis of Table III for bands overlapped by N I lines at 100 eV. However, due to threshold effects and energy uncertainties of ~0.5–1 eV at 20 eV for the spectral measurements, this ratio can vary between 0.25 and 0.6 from high- to low-v' levels. The modified-Born-approximation model described in the next section accounts for the threshold effect.

Table III gives the absolute emission cross section of the $b'(16,0)$ band as 2.14×10^{-19} cm^2 at 100 eV. We

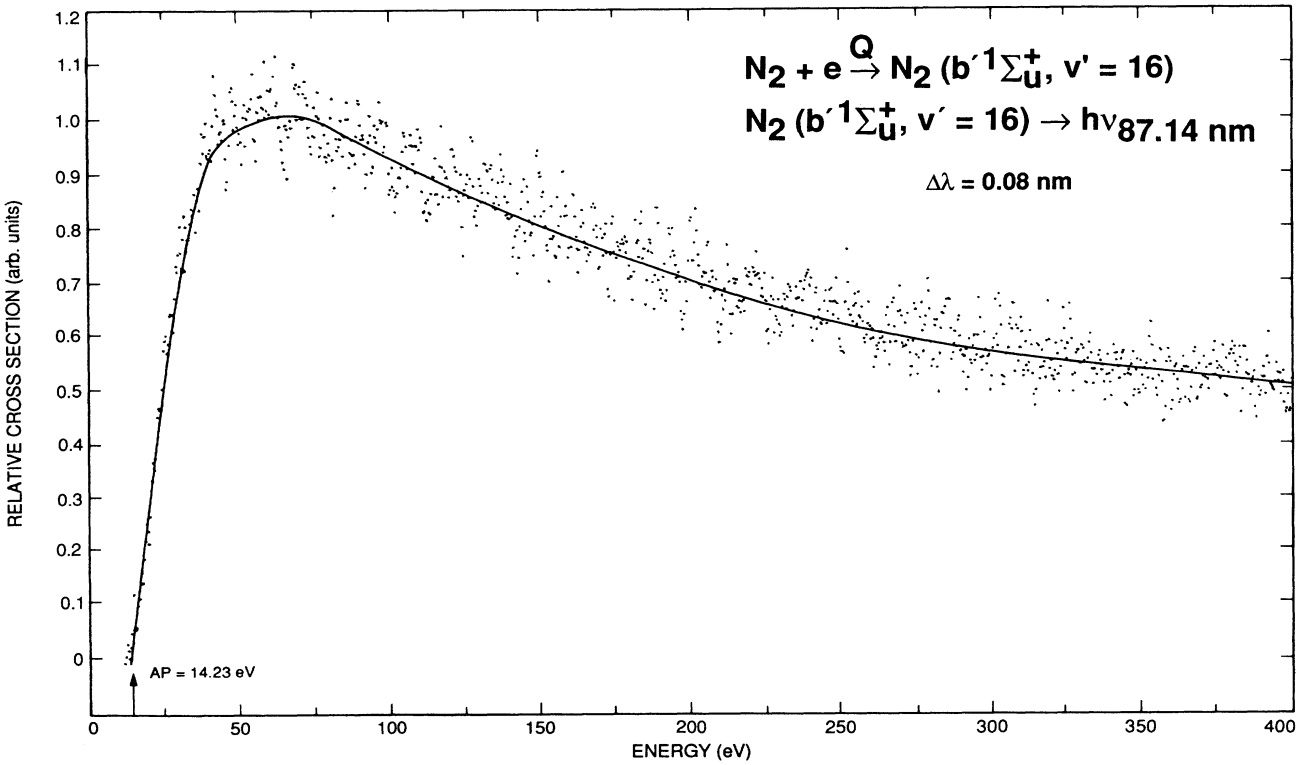

FIG. 16. Relative emission cross section of the $b'(16,0)$ vibrational band from 0 to 400 eV. Data points are obtained every 0.4 eV.

TABLE VI. Relative cross section $b'\,^1\Sigma_u^+(16) \rightarrow X\,^1\Sigma_u^+(0)$ band. $\Delta\lambda = 0.08$ nm, $\lambda = 87.14$ nm, and threshold = 14.23 eV. Measured (16,0) emission cross section at 100 eV 2.14×10^{-19} cm^2.

Energy (eV)	Cross section (arb units)	Energy (eV)	Cross section (arb. units)
14.23	0.00	70	0.99
16	0.06	80	0.98
18	0.16	90	0.95
20	0.28	100	0.92
22	0.39	120	0.89
25	0.47	150	0.82
30	0.66	200	0.71
35	0.79	250	0.62
40	0.88	300	0.57
50	0.96	350	0.54
60	1.00	400	0.51

have previously inferred a total emission cross section of the b' state as 19.9×10^{-19} cm^2. The ratio of the 65 to 100 eV emission cross sections is 1.05. Thus the peak emission cross section of the b' state is 20.9×10^{-19} cm^2.

The modified Born approximation to the collision strength for the $v' = 16$ vibrational level of the b' state is shown in Fig. 17. The accuracy of the fit to the data is better than 5%. It is based on the optical oscillator strength of 0.321 for the b' electronic state deduced by this experiment. The optical oscillator strength was found by equating the $v' = 11$ emission cross section to the $v' = 11$ excitation cross section. (Equivalently, we can also use $v' = 9$ level.) This procedure depends on the fact that the excitation cross section is greater than the emission cross section. We find that $v' = 11$ and 9 have the largest emission cross section to excitation cross section ratio and furnish the limiting constraint since this ratio must be less than unity for each vibrational level. At the limit, our oscillator strength for the b' system is nearly identical to the value of 0.311 deduced by Zipf and McLaughlin.[18] We find $v' = 9$ and 11 levels are virtually unpredissociated. The $v' = 11$ level emission cross section has only a small contribution from overlapped bands. A discussion in the next section shows that the oscillator strengths of Ref. 10 are about 33% too small for both the c_4' and b' states to account for the observed emission.

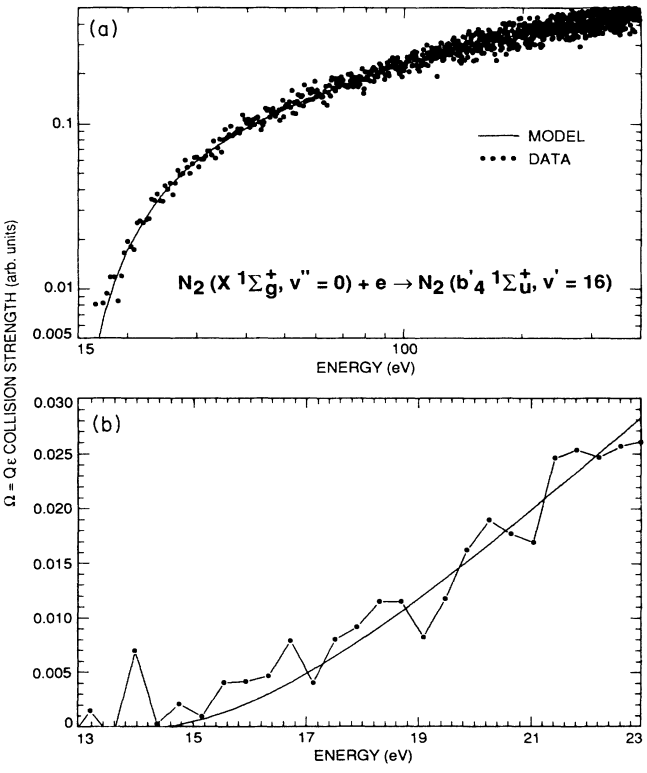

FIG. 17. Collision strength of the $b'\,^1\Sigma_u^+(16)$ vibrational level model (solid line) and data (dots) plotted against energy and normalized to an oscillator strength of 0.067 79 from Table VII(b) for $v' = 16$ (a) 13–400 eV and (b) 13–23 eV.

The experimental Franck-Condon factor for $v' = 16$ is obtained from the nearly identical relative intensity data of Refs. 2 and 18. These references show that the $v' = 16$ level contributes 21.3% of the total oscillator strength. The modified-Born-approximation formula can be used to determine the $v' = 16$ cross section to arbitrarily high energy. The constants for the Born-approximation model for all vibrational levels are given in Table VII. It is the basis of the excitation cross sections given in Table III(a). The $v' = 16$ excitation cross section is found to be 26.7×10^{-19} cm^2 at 100 eV. This cross section is 37% less than the corresponding value of 38.3×10^{-19} cm^2 from the work of Ref. 18, which we have extrapolated to 100 eV by use of the energy dependence in Table VI.

DISCUSSION

We have measured the emission spectrum of N_2 in the euv by electron impact at higher resolution and lower foreground abundance than in previous studies. The principal spectral measurements were conducted at 20 and 100 eV. With the spectral measurements and excitation-function measurements from 0 to 400 eV it was possible to make a comparison of absolute excitation and emission cross sections of the c_4' and b' states. The spectral measurements of band intensities were made possible with the recent high-resolution identifications of Roncin, Launay, and Yoshino.[17] The excitation-cross-section measurements of the c_4' state were made possible with the availability of the optical oscillator strengths[10,18] and the development of the modified-Born-approximation procedure.[22] There are no accurate lifetime measurements or absorption oscillator-strength measurements of the b' state available for use with the Born approximation.[12] To our knowledge there are no measurements of these quantities for the b' state subsequent to the Lofthus and Krupenie[12] review of 1973.

Previous electron-impact studies[18,19] have only used selected bands, some of which were shown to be incorrectly identified. By summing the cross-section contributions from all the vibrational bands we are able to calculate to 25% accuracy the electronic-emission cross section. Without any assumptions on the distribution of vibrational cross sections on the basis of Franck-Condon

approximation, "all the photons" in each progression were summed to give the total emission cross section and experimental $(v',0)$ Franck-Condon factors. Once the emission cross section was determined a comparison to the excitation cross section showed that the b' state was highly predissociated and that the c_4' was subject to negligible predissociation. Finally, we have measured, for the first time, the emission cross sections of the strongest vibrational bands of the higher Rydberg-series members of the $np\sigma$ $(n=5,6)$ and $np\pi$ $(n=4,5)$ Rydberg series.

The most important band for euv spectroscopic diagnostics of an N_2 atmosphere or gaseous regime undergoing electron excitation is the $c_4'(0,0)$ band. The cross section of the $c_4'(0,0)$ band has been measured and verified by two different methods. Previous measurements[18,19] of the strong $c_4'(0,0)$ band were in considerable error without the Lyman-α calibration standard correction. We compare in Table I the results of Huschilt, Dassen, and McConkey,[21] Zipf and McLaughlin,[18] and Morgan and Mentall[19] with our own. We have corrected these latter two works for the new calibration standard in the vuv for Lyman-α.[26,27] Our emission cross section for the (0,0) transition is 60.9×10^{-19} cm^2 at 200 eV. This value compares to 68.1×10^{-19} cm^2 from Zipf and McLaughlin and 31.1×10^{-19} cm^2 for Morgan and Mentall. The absolute cross section of Huschilt, Dassen, and McConkey was determined by normalizing their excitation function to theory.

For other features in this spectral range listed in Table I Morgan and Mentall[19] and Aarts and De Heer[20] have measured a few bands and emission lines. The comparison with Morgan and Mentall shows strong disagreement. Differences of a factor of 2 or more are typical. For the few comparisons possible with Aarts and De Heer the agreement is good for wavelengths longer than 100 nm, and differences approaching a factor of 2 below 100 nm probably arise from calibration techniques in the euv. The agreement of our work with McLaughlin[49] seems to be the best of the previous emission studies.

The only absolute experimental measurements of the excitation cross section were the electron-energy-loss measurements reported by Chutjian, Cartwright, and Trajmar[34] and Zipf and McLaughlin.[18] Chutjian, Cartwright, and Trajmar find a cross section of 88.0×10^{-19} cm^2 at 60 eV for the c_4' state. Our value for the c_4' state at this energy is 119×10^{-19} cm^2. However, the agreement between the two techniques is acceptable considering the $\pm50\%$ error bars reported by Chutjian, Cartwright, and Trajmar for the integral cross section. Extrapolations of the strongly forward-peaked differential cross section to small scattering angle lead to large uncertainties in the integral cross section. On the other hand, Zipf and McLaughlin report an excitation cross section of 201×10^{-19} cm^2 for the c_4' state at 200 eV. Of this total they attribute 158×10^{-19} cm^2 to the $c_4'(0)$ excitation cross section. Their analysis required the same extrapolations to small scattering angle as that of Chutjian, Cartwright, and Trajmar and one would expect similar large uncertainties by this technique. We believe that the major cause of the difference between the two experiments is the estimated values for the system oscillator strengths discussed below. To put the large difference in perspective, our estimate for the total emission cross section for the c_4' state at 200 eV is 98×10^{-19} cm^2. Of this amount we attribute 72×10^{-19} cm^2 to the $c_4'(0)$ level at 200 eV.

A recent review by Fox and Victor[50] deals with electron energy loss in N_2. The need to have available the predissociation cross section as one of the channels for electron energy loss is an important consideration in the modeling. This calculation requires both accurate emission and excitation cross sections. In order to avoid double-counting processes it is necessary to know the final states of the products in the total dissociation-cross-section measurements of Winters.[51] For example, we find the predissociation cross section of the b' state at 100 eV is 108×10^{-19} cm^2. The total dissociation cross section of N_2 at 100 eV is 2×10^{-16} cm^2.[51] Thus the b' state accounts for 5.4% of the dissociation of N_2 at 100 eV. Many of the results of Fox and Victor may have to be revised in light of the reduced cross sections for emission reported here. For example, use of the Zipf and McLaughlin c_4' emission cross sections with our Lyman-α revision leads them to erroneously conclude that the c_4' state is 50% dissociated for $0\le v'<4$. They also point out that using the available predissociation cross sections for the singlet states available at the time of their publication predissociation from the Rydberg and valence states accounts for up to 75% of the total dissociation. With our results from this paper and Ref. 3, an improved estimate will be possible.

We list in Table VII(a) a summary of cross-section coefficients, emission and excitation cross sections, and predissociation yields η for each vibrational level of the c_4' [Table VII(a)] and b' states [Table VII(b)]. Energy values are from Ref. 10. With this table it is possible to construct for any vibrational level at any arbitrary energy the emission and excitation cross section for modeling laboratory and planetary atmosphere data. Perhaps one of the most salient results of this study is the agreement of system oscillator strengths for the b' state with that of Ref. 18 and the strong disagreement with Ref. 10. Reference 18 finds for the b' state a system oscillator strength of 0.311 compared to our value of 0.321. Reference 10 deduces a system oscillator strength of 0.209 based on the laboratory data of Ref. 2 and the optical oscillator strength of Lawrence, Mickey, and Dressler[23] for the $b(4,0)$ band. Our value for the system oscillator strength of c_4' of 0.220 is halfway between the system oscillator strength of Ref. 18 at 0.316 and Ref. 10 at 0.139. Our results suggest a normalization problem for Ref. 10 since our results find a b' to c_4' ratio of about 1.44, in agreement with Ref. 10. However, Lawrence, Mickey, and Dressler claim a 20% accuracy to the $b(4,0)$ oscillator strength. Dressler[52] has pointed out to us that our f_0 value from Eq. (10) cannot be compared directly to the values of Stahel, Leoni, and Dressler. The Stahel, Leoni, and Dressler values for oscillator strengths are based on the adiabatic approximation of fixed internuclear distance and the strong c'-X bands with $v'=3,4,6,7$ borrow all their intensity from the b'-X levels.

The predissociation transition probability out of the b'

TABLE VII. Molecular parameters for modified Born approximation.

v'	$\bar{\nu}$ (cm^{-1})	$E_{ov'}$ (Ry)	$q_{v'o}$	$A(v,0)$[a] (ns^{-1})	$f_{ov'}$	C_7 (a.u.)	Q_{em} (100 eV) (10^{-19} cm^2)	Q_{ex} (100 eV) (10^{-19} cm^2)	η
				(a) N_2 ($c_4'-X$) molecular parameters					
0	104 323.30	0.950 781	0.718	1.140	0.1567	0.6592	88.8	88.8	0.000
1	106 369.50	0.969 430	0.017	0.029	0.0038	0.015 85	2.1	2.1	0.000
2	108 545.00	0.989 257	0.012	0.021	0.0027	0.010 749	1.4	1.4	0.000
3	110 657.20	1.008 507	0.059	0.111	0.0136	0.053 87	6.9	6.9	0.000
4	112 768.90	1.027 753	0.121	0.243	0.0285	0.1111	14.0	14.0	0.000
5	114 830.20	1.046 539	0.000	0.000	0.0000	0	0.0	0.0	0.000
6	116 806.80	1.064 553	0.073	0.163	0.0179	0.06732	8.2	8.2	~0.000
7	118 765.90	1.082 408	0.000	0.000	0.0000	0	0.0	0.0	
Total:			1.000		0.223		121.4	121.4	

$C_1/C_7=-0.086\,083$, $C_2/C_7=0.026\,813$, $C_3/C_7=-0.007\,754$, $C_4/C_7=-0.263\,79$, $C_5/C_7=-0.781\,22$, $C_6/C_7=0.781\,29$, $C_8=0.123\,03$, $C_0=0.0$.

$A(0,0)=1.140\ ns^{-1}$ $f_{00}=0.157$ $\omega_{00}=0.84$
$A(0,1)=0.188\ ns^{-1}$ $f_{10}=0.0273$ $\omega_{01}=0.14$
$A(0,2)=0.0183\ ns^{-1}$ $f_{20}=0.0027$ $\omega_{02}=0.014$
$A(0,3)=0.0041\ ns^{-1}$ $f_{30}=0.000\,64$ $\omega_{03}=0.0030$
$A(0)=1.350\ ns^{-1}$

Modified Born equation:[b]

$$\Omega(X)=C_0(1-1/X)(1/X^2)+\sum_{n=1}^{4} C_n(X-1)\exp(-nC_8X)+C_5+\frac{C_6}{X}+C_7\ln X,\quad X=\frac{E}{E_{ov'}}.$$

				(b) N_2 ($b'-X$) molecular parameters					
0	103 670.8	0.944 834	0.000 00	0	0	0.00			
1	104 418.7	0.951 651	0.000 00	0	0		0.000		
2	105 151.6	0.958 330	0.000 00	0	0		0.000		
3	105 869.2	0.964 870	0.000 00	0	0	1.000	1.000		
4	106 646.9	0.971 958	0.000 00	0	0		0.000		
5	107 326.7	0.978 154	0.000 45	0.000 135	0.000 554	0.060	0.060		
6	107 999.3	0.984 284	0.008 74	0.002 649	0.010 766	0.510	1.160	0.560	
7	108 950.8	0.992 955	0.011 14	0.003 409	0.013 734	1.470	1.470		
8	109 544.1	0.998 363	0.006 85	0.022 107	0.008 442	0.650	0.900a		
9	110 197.4	1.004 317	0.030 80	0.009 529	0.037 954	3.900	4.029	0.032	
10	110 942.3	1.011 105	0.005 28	0.001 643	0.006 501	0.190	0.687	0.723	
11	111 581.3	1.016 929	0.011 18	0.003 504	0.013 783	1.450	1.450	0.000	
12	112 238.2	1.022 916	0.096 13	0.030 297	0.118 475	2.980	12.406	0.760	
13	112 908.5	1.029 025	0.014 01	0.004 443	0.017 271	0.320	1.801	0.822	
14	113 539.2	1.034 773	0.131 18	0.041 825	0.161 680	1.060	16.786	0.937	
15	114 170.2	1.040 524	0.171 25	0.054 902	0.211 058	0.460	21.822	0.979	
16	114 754.5	1.045 849	0.210 37	0.067 792	0.259 281	5.260	26.705	0.803	
17	115 369.6	1.051 455	0.114 66	0.037 148	0.141 320	0.240	14.497	0.983	
18	116 206.6	1.059 083	0.010 32	0.003 366	0.012 713	0.160	1.297	0.877	
19	116 682.8	1.063 423	0.065 62	0.021 500	0.080 871	0.150	8.225	0.982	
20	117 205.2	1.068 184	0.055 82	0.018 373	0.068 801		6.974	1.000	
21	117 681.3	1.072 523	0.000 00	0	0		0.000		
22	118 485.4	1.079 852	0.016 63	0.005 532	0.020 493		2.060	1.000	
23	118 968.4	1.084 254	0.028 17	0.009 411	0.034 720		3.479	1.000	
24	119 430.8	1.088 468	0.011 40	0.003 823	0.014 051		1.404	1.000	
25	119 834.3	1.092 145	0.000 00	0	0		0.000		
Total:			1.000 00		0.321	19.9	128.2		

$C_1/C_7=0.168\,09$, $C_4/C_7=0.985\,118$, $C_5/C_7=-1.507\,258$, $C_6=-C_5$, $C_8=0.234\,42$, $C_0=C_2=C_3=0.0$.

[a]Assumes no predissociation.
[b]References 22 and 26.

state is dependent on the vibrational level. In general, predissociation increases with quantum number, although higher-resolution measurements are needed to quantify the individual v' progressions. The published analysis of Zipf and McLaughlin[18] for the b' state shows a predissociation rate of 83% for the b' state. Our analysis shows a predissociation rate of 84% for the entire electronic transition. The close agreement between the work of Ref. 18 and the work presented here for the predissociation rate is fortuitous. A correction of 0.62 is applied to the emission cross sections of Ref. 18 to account for the Lyman-α calibration correction; a correction factor of 0.67 is applied to the excitation cross sections of Ref. 18 to bring the optical oscillator strengths into agreement with recent measurements and theory. Thus correcting the Ref. 18 b' emission cross section by a factor of 0.62 at 200 eV yields a cross section of 20×10^{-19} cm^2. Our cross section at 200 eV is 13.3×10^{-19} cm^2, barely within the experimental uncertainty. Part of the remaining discrepancy in the case of the b' state between Ref. 18 and the work presented here is that Ref. 18 identified many of their features between 92 and 95 nm as weak underlying b' bands rather than the stronger c'_4 bands.

The strongest b' band in emission is the $b'(16,0)$ band compared to the (14,0) in absorption (Yoshino[53]). The breaking off of the bands at $v'=20$ found in this experiment is an important result confirming strong predissociation for $v'>19$.

We have been able to estimate the total emission cross section for the c'_4 state by summing the emission cross sections in our high-resolution spectra. Features that were not resolved contribute very little to the total cross section. For example, we find in Table II that the uncertainty in the total cross section at 100 eV from unresolved bands is 4×10^{-19} cm^2 out of a total cross section of 120×10^{-19} cm^2. The branching of the $c'_4(0)$ vibrational level to the $a\ ^1\Pi_g$ state has a maximum emission cross section of 1×10^{-19} cm^2 near 70–80 eV.[54] The branching ratios of the $c'_4(0)$ level are 1.1% to the $a\ ^1\Pi_g$ state and 98.9% to the $X\ ^1\Sigma_g^+$ ground state. In single-scattering processes involving the c'_4 state only radiation processes to the ground state are important in energy transfer. At the same time it must be remembered that the $c'_4(0)$-$a(v'')$ bands have been identified in the terrestrial aurora by Slanger[55] for $v''=4,5$. These results would imply the c'_4-X band system should be easy to detect in the Earth's atmosphere.

The relative band intensities in Table II are in good agreement with the results of Geiger and Schroder[2] and indicate that predissociation for the c'_4 vibrational levels is small, certainly less than 10%. Since absorption experiments have noted sharp features, at least at the limit of their instrumental resolution, the predissociation lifetime out of the $c'_4(v')$ levels must be greater than 10^{-2} times the radiative lifetime; i.e., "weak predissociation" is indicated. The absorption experiment of Yoshino and Tanaka[7] at a resolution of 5 mA for the $c'_4(0,0)$ band would have been able to detect diffuseness for predissociation lifetimes of less than 10^{-11} s. For a radiative lifetime of 0.9×10^{-9} s for the $c'_4(0)$ level and a 0.84 branching ratio to the (0,0) band an upper limit of 98.7% predissociation is ascertained by the high-resolution absorption-spectroscopy results. Our electron-impact results imply a more stringent result that predissociation must be less than 10%. At the present time no experimenter has performed the 1-mA measurement required for studying the rotational line shapes for the $c'_4(0,0)$ band. The point where the predissociation width is larger than the Doppler width occurs for a predissociation lifetime of 5×10^{-11} s and can be used as the criterion to distinguish "weak" and "strong" predissociation. This value occurs at 94% predissociation yield. Any predissociation yield of less than 94% is a weak predissociation. This point is reaffirmed for the b' state where the predissociation yield of the state is 84%. Both the b' and c'_4 states satisfy the criterion for weak predissociations.

The absence of measurable predissociation in the c'_4-X band system in the laboratory raises a fundamental problem for the Earth aeronomers. N_2, the most abundant species in the Earth's atmosphere at 120 km, where many of the dayglow and auroral processes take place, shows scant evidence of c'_4 vibrational band emissions in the euv. Aeronomers[18,55–57] theorize that some unknown, and negligibly small predissociation is responsible for the absence of appreciable $c'_4(0,0)$ band emission at 95.8 nm. We cannot at the present time discount this possibility. The atmosphere may be the most sensitive "laboratory" test for a small process that is amplified 10^4 by self-absorption. Other more likely possibilities based on this work are cascading to the $a\ ^1\Pi_g$ state and fluorescence in the (0,1),(0,2), . . . , bands.[55–57] However, aeronomers maintain that the airglow and aurora radiation do not come out in the longer-wavelength members of the $v'=0$ progression or in the LBH bands. Another effect of the known weak interaction between $b'(1)$ and $c'(0)$ on the emission spectrum has not been taken into account and may also be important in explaining the lost energy. Stahel, Leoni, and Dressler[10] calculate that the percentage b' character in the $c'_4(0)$ level for $J=0$ is about 1% from the $v'=0$ and 1 vibrational levels. Perhaps fluorescence from the $b'(1)$ or $b'(0)$ progressions should be looked for in the Earth's atmosphere. Some of the most recent data showing that the rich spectra observed from observing the Earth's atmosphere have been acquired by Chakrabarti *et al.*,[41] Paresce *et al.*,[43] and Gentieu *et al.*[42] The principal difficulty in the rocket and satellite measurements is the lack of spectral resolution to separate the weaker N_2 bands from the prevalent atomic O emissions. The highest-resolution emission spectrum in the euv was obtained by Gentieu *et al.*[42] with a spectral resolution of 0.3 nm. They use the original cross sections of Zipf and McLauglin[18] for the b' and c'_4 states, which are in error by nearly a factor of 2. The factor of 2 would account for most of the "missing" photons from the spectral analysis of the euv dayglow according to Gentieu *et al.* The limb spectrum of Gentieu *et al.* also clearly shows evidence for $c'_4(0,v''\geq1)$ vibrational bands. Reanalysis of the Gentieu *et al.* data may be warranted with the emission cross sections, identifications, and $(v',0)$ Franck-Condon factors presented here. Recent unpublished 0.2-nm resolution spectra of Feldman[58] for

the dayglow represent the highest-resolution spectra of the earth's atmosphere and clearly show the $c_4'(0,v'')$ progression. It seems likely for the Earth that a variety of processes can effectively spread the optically thick (0,0) band radiation over many vibrational bands from 96 to 110 nm. For example, this may account for the failure to see an enhancement in the $c_4'(0,1)$ band by the pressure line linearity test in Fig. 3. Park, Feldman, and Fastie[59] have pointed out that the N_2 molecular emissions will appear as a broadband continuum in the low-resolution rocket spectra. Laboratory measurements of high-resolution spectra and experimental Franck-Condon factors will provide a guide for aeronomers in the analysis of the observations of dayglow and aurora, which until now have been unavailable.

On the other hand, the atmosphere of Titan was identified as having N_2 as a principal constituent because of the easily discernable and strong 95.8-nm, $c_4'(0,0)$, emission.[40] Evidently the electron-impact process took place high enough in the atmosphere that self-absorption was not important in the Voyager observation. Analysis of the Voyager Titan data has awaited the more accurate cross sections presented here.

In general, this work complements Roncin, Launay, and Yoshino's analysis at low pressure of emission bands, since only the electron-beam work at very low pressure is capable of observing the resonance transitions in emission. Bands in the euv spectrum of N_2 produced by electron-impact fluorescence from high Rydberg states have been identified. In particular, weak $c_4\ ^1\Pi_u$, $c_5\ ^1\Pi_u$, $c_5'\ ^1\Sigma_u^+$, $c_6'\ ^1\Sigma_u^+$, and $o\ ^1\Pi_u$ vibrational bands were detected between 82 and 91 nm. In Ref. 3, we plan to discuss electron-impact excitation of the $b\ ^1\Pi_u$ Rydberg state and the importance of predissociation and vibrational perturbations for this band system in relation with the $o_n\ ^1\Pi_u$ and $c_n\ ^1\Pi_u$ band systems.[4,60]

ACKNOWLEDGMENTS

This work was supported by the U.S. Air Force Office of Scientific Research (AFOSR), the Aeronomy Program of the National Science Foundation Grant No. ATM 8715709, and NASA Planetary Atmospheres and Astronomy/Astrophysics Program Offices, under Contract No. NAS7-100 to the Jet Propulsion Laboratory, California Institute of Technology, and Contract No. NAGW-649 to the University of Arizona. We have greatly benefited from conversations with and careful readings of the manuscript by F. Launay, H. Lefebvre-Brion, J.-Y. Roncin, K. Yoshino, G. Victor, and P. Cosby.

[1]P. K. Carroll and Kh. I. Hagim, Phys. Scr. **37**, 682 (1988).
[2]J. Geiger and B. Schroder, J. Chem. Phys. **50**, 7 (1969).
[3]G. K. James, J. M. Ajello, B. O. Franklin, and D. E. Shemansky (unpublished).
[4]P. K. Carroll and C. P. Collins, Can. J. Phys. **47**, 563 (1969).
[5]P. K. Carroll, C. P. Collins, and K. Yoshino, J. Phys. B **3**, L127 (1970).
[6]K. Yoshino, D. E. Freeman, and Y. Tanaka, J. Mol. Spectrosc. **76**, 153 (1979).
[7]K. Yoshino and Y. Tanaka, J. Mol. Spectrosc. **66**, 219 (1977).
[8]P. K. Carroll and K. Yoshino, J. Phys. B **5**, 1614 (1972).
[9]G. Herzberg, *Molecular Spectra and Molecular Structure I, Spectra of Diatomic Molecules* (Van Nostrand, New York, 1950), p. 292.
[10]D. Stahel, M. Leoni, and K. Dressler, J. Chem. Phys. **79**, 2541 (1983).
[11]K. P. Huber and G. Herzberg, *Molecular Spectra and Molecular Structure IV, Constants of Diatomic Molecules* (Van Nostrand Reinhold, New York, 1979), p. 420.
[12]A. Lofthus and P. H. Krupenie, J. Phys. Chem. Ref. Data **6**, 113 (1977).
[13]K. Dressler, Can J. Phys. **47**, 547 (1969).
[14]H. Lefebvre-Brion, Can. J. Phys. **47**, 541 (1969).
[15]H. Lefevbre-Brion, R. W. Field, *Perturbations in the Spectra of Diatomic Molecules* (Academic, Orlando, 1986), Chap. 5, p. 244.
[16]K. Yoshino and D. E. Freeman, Can. J. Phys. **62**, 1478 (1984).
[17]J.-Y. Roncin, F. Launay, and K. Yoshino, Planet. Space Sci. **35**, 267 (1987); J. Mol. Spectrosc. (to be published).
[18]E. C. Zipf and R. W. McLaughlin, Planet. Space Sci. **26**, 449 (1978).
[19]H. D. Morgan and J. E. Mentall, J. Chem. Phys. **78**, 1747 (1983).
[20]J. F. M. Aarts and F. J. De Heer, Physica **52**, 45 (1971).
[21]J. C. Huschilt, H. W. Dassen, and J. W. McConkey, Can. J. Phys. **59**, 1893 (1981); J. L. Forand, S. Wang, J. M. Woolsey, and J. W. McConkey, *ibid.* **66**, 349 (1988).
[22]D. E. Shemansky, J. M. Ajello, D. T. Hall, and B. Franklin, Astrophys. J. **296**, 774 (1985).
[23]G. M. Lawrence, D. L. Mickey, and K. Dressler, J. Chem. Phys. **48**, 1989 (1968).
[24]J. Hesser and K. Dressler, J. Chem. Phys. **45**, 3149 (1966).
[25]S. K. Srivastava, A. Chutjian, and S. Trajmar, J. Chem. Phys. **63**, 2659 (1975); S. Trajmar and D. Register, in *Electron Molecular Collisions,* edited by K. Takayanagi and I. Shimamura (Plenum, New York, 1984), Chap. 6.
[26]D. E. Shemansky, J. M. Ajello, and D. T. Hall, Astrophys. J. **296**, 765 (1985).
[27]K. D. Pang, J. M. Ajello, B. Franklin, and D. Shemansky, J. Chem. Phys. **86**, 2750 (1987).
[28]S. G. Tilford and P. G. Wilkinson, J. Mol. Spectrosc. **12**, 231 (1964).
[29]P. G. Wilkinson and N. B. Houk, J. Chem. Phys. **24**, 528 (1956).
[30]J.-Y. Roncin, F. Launay, and M. Larzilliere, Phys. Rev. Lett. **53**, 159 (1984).
[31]M. J. Mumma and E. C. Zipf, J. Chem. Phys. **55**, 5582 (1971).
[32]H. Helm and P. C. Cosby, J. Chem. Phys. (to be published).
[33]E. N. Lassettre, Can. J. Chem. **47**, 1733 (1969).
[34]A. Chutjian, D. C. Cartwright, and S. Trajmar, Phys. Rev. A **16**, 1051 (1977).
[35]J. M. Ajello and D. E. Shemansky, J. Geophys. Res. **90**, 9845 (1985).
[36]J. M. Ajello, D. E. Shemansky, B. Franklin, J. Watkins, S. Srivastava, G. K. James, W. T. Simms, C. W. Hord, W. Pryor, W. McClintock, V. Argabright, and D. Hall, Appl.

Opt. **27**, 890 (1988).
[37]J. M. Ajello, D. Shemansky, T. L. Kwok, and Y. L. Yung, Phys. Rev. A **29**, 636 (1984).
[38]G. K. James, J. M. Ajello, D. E. Shemansky, B. Franklin, D. Siskind, and T. G. Slanger, J. Geophys. Res. **93**, 9893 (1988).
[39]P. M. Banks and G. Kockarts, *Aeronomy Part A* (Academic, New York, 1973), p. 5.
[40]D. F. Strobel and D. E. Shemansky, J. Geophys. Res. **87**, 1361 (1982).
[41]S. Chakrabarti, F. Paresce, S. Bowyer, R. Kimble, and S. Kumar, J. Geophys. Res. **88**, 4898 (1983).
[42]E. P. Gentieu, P. D. Feldman, R. W. Eastes, and A. B. Christensen, Geophys. Res. Lett. **8**, 1242 (1981).
[43]F. Paresce, S. Chakrabarti, S. Bowyer, and R. Kimble, J. Geophys. Res. **88**, 4905 (1983).
[44]S. Chakrabarti, J. Geophys. Res. **91**, 8065 (1986).
[45]R. T. Brinkmann and S. Trajmar, J. Phys. E **14**, (1981).
[46]R. L. Kelly and L. J. Palumbo, *Atomic & Ionic Emission Lines Below 2000 Angstroms* (Naval Research Laboratory, Washington, D.C., 1973), p. 26; R. Kelly, J. Phys. Chem. Ref. Data **16**, 53 (1987).
[47]R. E. Worley, Phys. Rev. A **64**, 207 (1943).
[48]J. M. Ajello, J. Chem. Phys. **55**, 3158 (1971).
[49]R. W. McLaughlin, Ph.D. thesis, University of Pittsburgh, 1977.
[50]J. L. Fox and G. A. Victor, Planet. Space Sci. **36**, 329 (1988).
[51]H. F. Winters, J. Chem. Phys. **44**, 1472 (1965).
[52]K. Dressler (private communication).
[53]K. Yoshino (private communication).
[54]A. R. Filippelii, S. Chung, and C. C. Lin, Phys. Rev. A **29**, 1709 (1984); J. S. Allen and C. C. Lin, *ibid.* **39**, 383 (1989).
[55]T. G. Slanger, Planet. Space Sci. **31**, 1525 (1983).
[56]P. D. Feldman and E. P. Gentieu, J. Geophys. Res. **87**, 2453 (1982).
[57]R. R. Conway, J. Geophys. Res. **88**, 4784 (1983).
[58]P. Feldman (private communication).
[59]H. Park, P. D. Feldman and W. G. Fastie, Geophys. Res. Lett. **4**, 41 (1977).
[60]K. Yoshino and Y. Tanaka, J. Mol. Spectrosc. **54**, 87 (1975).